HORIZON 2020

Nuclear Fission and Radiation Protection 2018 (NFRP-2018-4)

Project acronym:	**SANDA**
Project full title:	**Solving Challenges in Nuclear Data for the Safety of European Nuclear facilities**
Grant Agreement no.:	**H2020 Grant Agreement number: 847552**

Workpackage N°:	*WP2*
Identification N°:	*D2.12*
Type of document:	*Deliverable*
Title:	REPORT ON THE FISSION YIELD STUDIES WITH THE LOHENGRIN SPECTROMETER AT ILL
Dissemination Level:	*PU*
Reference:	
Status:	*VERSION 1*
Comments:	….

	Name	Partner	Date	Signature
Prepared by:	C. Sage	5		
WP leader:	D. Cano Ott	1		
IP Co-ordinator:	E. González	1		

Report_SANDA_Deliverable_D2.12

SANDA Project D2.12: Report on the fission yield studies with the LOHENGRIN spectrometer at ILL

A. Chebboubi[1], G. Kessedjian[1], O. Litaize[1], O. Serot[1], C. Sage[3], S. Julien-Laferriere[1,3], J. Nicholson[1], O. Méplan[3], D. Bernard[1], A. Blanc[2], H. Faust[2], Y.H. Kim[2], U. Köster[2], P. Mutti[2], M. Ramdhane[3], A. Letourneau[4], T. Materna[4], M. Rapala[4]

[1]CEA-Cadarache, DES, IRESNE, DER, SPRC, LEPh, F-13108 Saint Paul lez Durance (France).

[2]Institut Laue-Langevin, F-38042 Grenoble Cedex 9 (France).

[3]LPSC, Université Grenoble-Alpes, CNRS/IN2P3, F-38026 Grenoble Cedex (France).

[4]CEA-Saclay, DRF, Irfu, DPhN, LEARN, Orme des merisiers, F-91191 Gif sur Yvette (France).

Contact: christophe.sage@lpsc.in2p3.fr Tel: +33 4 76 28 41 34.

1. Introduction

This work is part of the 2.5.1 subtask "Fission yield studies in (n,f) reactions" and is coupled to the 4.2.1 subtask "Evaluation of fission yields".

Since 2007, the CEA-Cadarache, in collaboration with the Laboratoire de Physique Subatomique et Corpusculaire de Grenoble (LPSC/ CNRS) and the Laue-Langevin Institute (ILL) de Grenoble have developed a large experience in measuring, analyzing and evaluating thermal neutron-induced fission yields. In the framework of this collaboration, a program of actinide fission yield measurements of interest for the current and innovative nuclear reactors was initiated (see for example Ref. [Chebboubi 2021]). This program is of prime importance for many applications: estimation of the radionuclide inventories in nuclear fuel for decay heat calculation and spent fuel storage, radioprotection applications, depletion calculations in PWR cells….

Additionally, our experimental program involves a large range of observables requested to test some model assumptions implemented in the Monte-Carlo code FIFRELIN [Litaize 2015], which is a code used for fission yield evaluations.

Among these observables, two have been studied and are detailed in this 2.5.1 subtask report:

- Isotopic yield measurement as a function of the kinetic energy for the ^{241}Pu(n$_{th}$,f) reaction
- ^{132}Sn Isomeric ratio measurement as a function of the kinetic energy.

The main aim of these experiments is to test the sharing of the total excitation energy between both fission fragments and the spin generation mechanism. This information is the key observable for the evaluation of isotopic yields.

2. Kinetic energy dependency of isotopic distributions

The measurements were carried out using the LOHENGRIN mass spectrometer located at the ILL in Grenoble, France. The ^{241}Pu target was placed in a beam tube under a neutron flux of about 5×10^{14} n.cm^{-2}.s^{-1}. The emerging ionized fission products are deflected by an electromagnetic field. The ones with the same mass over ionic charge A/q and kinetic energy over ionic charge Ek/q ratios have the same trajectory. For the isotopic yields measurements, the fission products end up on a movable tape inside a vacuum chamber and surrounded by two clovers of four high purity germanium detectors, where the characteristic γ-ray energy for each isotope decay can be measured. The detailed measurement and analysis procedure was published in Ref. [Julien-Laferrière 2020a].

Fig. 1 shows the results obtained for the mass A=139 absolute isotopic yields produced from the thermal neutron induced fission of ^{241}Pu along with the associated covariance matrix. On the left is shown the case using the actual uncertainties of I$^{\gamma}$ (the γ transition intensity) and on the right is shown the case where the uncertainty of the normalization intensity I^{γ}_{Norm} is equal to zero. It shows that the uncertainties are mainly coming from nuclear decay data, since the total uncertainty is reduced by a factor of 4 for the latter.

FIFRELIN can compute the isotopic yields as a function of the fission product kinetic energy through an event-by-event analysis. However, the computed kinetic energy (after prompt neutron emission) needs to be corrected for the energy loss of fission products inside the target and its cover. To take this into account, FIFRELIN kinetic energy distributions are convoluted by a Landau distribution which models the energy loss of ions through a thin layer. This procedure is also detailed within Ref. [Julien-Laferrière 2020a].

Fig. 2 shows the results of such a comparison. The agreement between the experimental data and FIFRELIN is satisfactory even if a slight overestimation of FIFRELIN for Xe is observed. Indeed, all the experimental data (except the 54 MeV point for I) are compatible with FIFRELIN with a confidence level of 90%. In other words, FIFRELIN is validated in regards to the kinetic energy dependence of the mass A = 139.
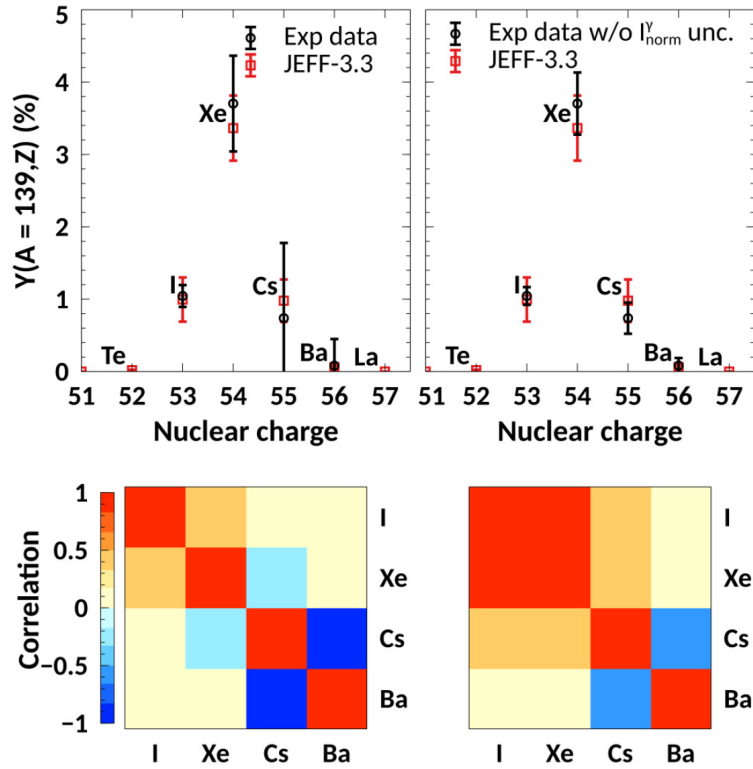
Figure 1: Absolute isotopic yields for the mass A = 139 with all the uncertainties propagated (left) and for the case where ΔI_{Norm}^{γ}=0 (right). A comparison with the JEFF-3.3 library is also displayed. Correlation matrices in both cases are also displayed (bottom) [Julien-Laferrière 2020a].
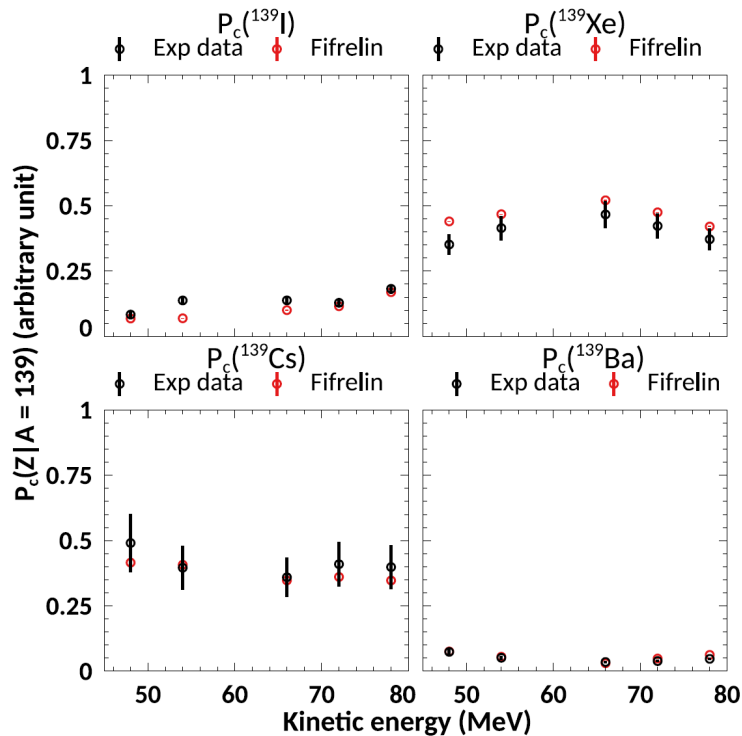
Figure 2: Relative cumulated isotopic yield probability for experimental data (black points) and FIFRELIN calculations after energy loss corrections (red points). The experimental kinetic energy refers to the LOHENGRIN selected energy, i.e., after the cover foil [Julien-Laferrière 2020a].

This work was part of the article published by S. Julien-Laferrière [Julien-Laferrière 2020a].

3. Kinetic energy dependency of isomeric ratios

Another experimental campaign performed on the LOHENGRIN spectrometer is related to the kinetic energy dependence of ^{132}Sn fission product isomeric ratio (IR) measured for thermal neutron induced fission of ^{241}Pu. This work was done in the frame of the PhD thesis of J. Nicholson [Nicholson 2021a]. The IRs are deduced using gamma ray spectrometry in coincidence with the signals of the ionization chamber. The isomeric ratio is defined as the ratio of the production rate of one isomeric state to the sum of the production rates of all the isomeric states and the ground state. The details of the measurement and analysis procedure can be found in Ref. [Nicholson 2021a - Nicholson 2021b].

Results obtained for ^{241}Pu(n$_{th}$,f) are shown in Fig. 3, and compared with a previous measurement campaign for ^{235}U(n$_{th}$,f) [Chebboubi 2017] in Fig. 4. In this figure, the ^{132}Sn kinetic energy distributions (after prompt neutron emission) are also shown.
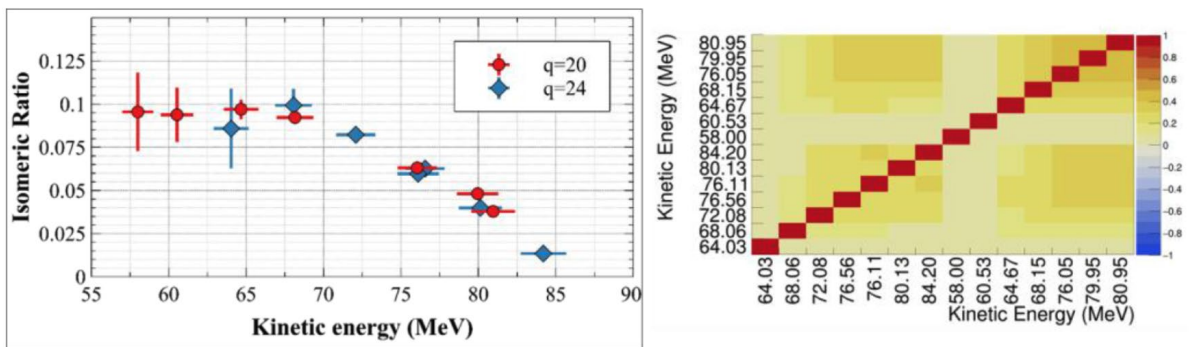
Figure 3: Isomeric Ratio of ^{132}Sn from thermal neutron induced fission of ^{241}Pu measured at two different ionic charge selections (left) and the associated covariance matrix (right). The kinetic energies are corrected from the relative evolution of the energy loss during the experimental campaign [Nicholson 2021b].
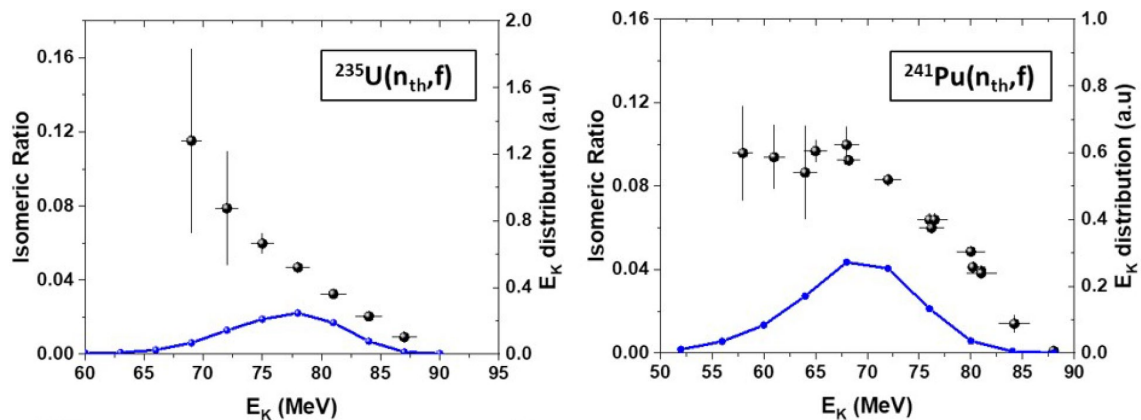
Figure 4: Isomeric Ratio of ^{132}Sn measured as a function of its kinetic energy (left scale, black points). The ^{132}Sn kinetic energy distribution is given by the blue curve (right scale). Left : results from the ^{235}U(n$_{th}$,f) reaction [6]. Right: results from the ^{241}Pu(n$_{th}$,f) reaction [Nicholson 2021a - Nicholson 2021b].

The interpretation of these data using the FIFRELIN Monte-Carlo code to simulate the de-excitation of the fission fragments is detailed within the deliverable D4.3 report of the Sanda project, where the angular momentum distribution with kinetic energy of the doubly magic nucleus of ^{132}Sn is deduced and discussed.

This work was done in the frame of the PhD thesis of J. Nicholson [Nicholson 2021a].

References

[Chebboubi 2021] A. Chebboubi *et al.*, *Measurements of U-233(n_{th}, f) fission product mass yields with the LOHENGRIN recoil mass spectrometer*. European Physical Journal A 57, (2021) 335.

[Litaize 2015] O. Litaize *et al.*, *Fission modelling with FIFRELIN*. European Physical Journal A 51, (2015) 177.

[Julien-Laferrière 2020a] S. Julien-Laferrière *et al., Investigation of neutron emission through the local odd-even effect as a function of the fission product kinetic energy.* Physical Review C 102, (2020) 034602

[Julien-Laferrière 2020b] S. Julien-Laferrière *et al., Fission fragments observables measured at the LOHENGRIN spectrometer.* European Physical Journal Web of Conferences 239, (2020) 05017

[Nicholson 2021a] J. Nicholson, PhD thesis, University Grenoble Alpes, Sept. 2021

[Chebboubi 2017] A. Chebboubi *et al.*, *Kinetic energy dependence of fission fragment isomeric ratios for spherical nuclei 132Sn*. Physical Letters B, 775, (2017) 190.

[Nicholson 2021b] J. Nicholson *et al., Investigation of fission product isomeric ratios and angular momenta of 132Sn populated in the 241Pu(nth,f) reaction*. European Physical Journal Web of Conferences 256, (2021) 00011

Investigation of neutron emission through the local odd-even effect as a function of the fission product kinetic energy

S. Julien-Laferrière,[1,2] A. Chebboubi ⬤,[1,*] G. Kessedjian,[2] O. Serot,[1] O. Litaize ⬤,[1] A. Blanc,[3]
U. Köster ⬤,[3] O. Méplan,[2] M. Ramdhane ⬤,[2] and C. Sage[2]

[1]*CEA, DES, IRESNE, DER, SPRC, Physics Studies Laboratory, Cadarache, F-13108 Saint-Paul-lès-Durance, France*
[2]*LPSC, Université Grenoble-Alpes, CNRS/IN2P3, F-38026 Grenoble Cedex, France*
[3]*Institut Laue-Langevin, F-38042 Grenoble Cedex 9, France*

A recent experimental campaign was completed at the LOHENGRIN spectrometer. It was dedicated to the determination of the local odd-even effect as a function of the fission product kinetic energy for a given mass. We discuss here the mass $A = 139$ produced from the thermal neutron induced fission of ^{241}Pu. A comparison with the Monte Carlo code FIFRELIN allows one to interpret these data in regards to the neutron emission process. The long term goal is to test and validate the phenomenological temperature ratio law used in FIFRELIN to split the total excitation energy between both fission fragments.

I. INTRODUCTION

Studies of new and current nuclear reactors rely increasingly on numerical tools. Because of the increase in computational power and the improvement of neutron transport codes, limits on precision are now shifting towards inputs derived from evaluated nuclear data. These evaluated data are a combination of experimental and theoretical knowledge. One way to improve such evaluated data is to perform more accurate measurements and develop more physical models. In this framework, the nuclear fission process [1,2] continues to challenge physicists despite being discovered 80 years ago. Plenty of models are available with different fundamental hypotheses to explain nuclear fission [3–10]. Several experimental fission observables have been studied such as mass and isotopic yields. Among these fission observables, an investigation of the local proton odd-even effect (after neutron emission) $\delta_Z(A)$ can be performed:

$$\delta_Z(A) = \frac{\sum_e Y(A, Z_e) - \sum_o Y(A, Z_o)}{Y(A)} \qquad (1)$$

where indices e and o correspond to even and odd parities respectively. The mass and isotopic yields (after neutron emission) are referred as $Y(A)$ and $Y(A, Z)$ respectively.

Moreover the dependence of $\delta_Z(A)$ on fission product kinetic energy could be used to deduce the total excitation energy sharing at scission between both fission fragments. Determination of the excitation energy repartition is essential in the calculation of the prompt neutron and gamma spectra. This observable is complementary to the isomeric ratio measurements as a function of the fission product kinetic energy [11].

In the past, the global proton odd-even effect δ_Z was investigated as a function of the fission product kinetic energy [12–14]. It showed that δ_Z increases with the fission product kinetic energy for the three reactions investigated [^{232}U (n_{th}, f), ^{233}U (n_{th}, f), ^{229}Th (n_{th}, f)].

In this article, we first introduce a new methodology for data taking and analysis of isotopic yield measurements with the LOHENGRIN spectrometer. It will be illustrated with the mass $A = 139$. Then, we report the measurement of the local odd-even effect as a function of the fission product kinetic energy for the mass $A = 139$ in the thermal neutron induced fission of ^{241}Pu.

II. EXPERIMENTAL SETUP

The $\delta_Z(A)$ measurement was carried out using the LOHENGRIN recoil separator for fission products [15] located at the high-flux reactor of Institut Laue-Langevin (ILL) in Grenoble, France. The fission target was placed in a beam tube under a neutron flux of about 5×10^{14} n cm^{-2}s^{-1}. In order to reduce the target self-sputtering and improve its burn-up behavior control [16], the target is covered by a thin nickel foil ($\approx$0.25 μm).

The emerging ionized fission products are first deflected by an horizontal magnetic field and then by a vertical electrostatic field. Note that the spectrometer operates under secondary vacuum ($\approx$10^{-6} mbar). Fission products with the same mass over ionic charge $\frac{A}{q}$ and kinetic energy over ionic charge $\frac{E_k}{q}$ ratios have the same trajectory. Finally, the last part of the LOHENGRIN spectrometer is a focusing magnet [17] that can be switched on or (switched) off. It allows us to reach two experimental positions to disentangle the selected triplets (A, q, E_k). The "straight" position enables one to measure the mass yields by using a double anode Frisch grid ionization chamber (IC) as a detector. The "curved" position takes

Report_SANDA_Deliverable_D2.12_Julien-Laferriere_2020a

advantage of the second magnetic field to increase particle density at the focal plane position. In other words, it refocuses ions with different kinetic energies and deflects them towards an array of detectors. In this case, fission products end up on a movable tape (inside a vacuum chamber) surrounded by two clovers. Each clover contains four high purity germanium (HPGe) detectors. It is designed to calculate the isotopic yields by measuring the characteristic γ-ray energy for each isotope decay. Shown results mainly come from the "curved" position setup. Note that all quantities used in the following (kinetic energy, mass, etc.) correspond to post neutron emission quantities unless otherwise specified.

III. DATA TAKING AND ANALYSIS

The local odd-even effect depends directly on the isotopic and mass yields. In this section, descriptions of mass and isotopic yield measurements are shown. More details can be found in Refs. [18–21].

A. Mass yield

As previously explained, the LOHENGRIN spectrometer selects triplets (A, E_k, q). To detect the mass of the incoming ions, an IC is used at the "straight" position to measure the kinetic energy and therefore the associated mass. The number of counts $N(A, q, E_k \pm \frac{\Delta E_k}{2}, \Delta t_m, t)$ extracted from the IC depends on the mass A, the ionic charge q, the kinetic energy E_k, the LOHENGRIN energy resolution ΔE_k, the measurement time Δt_m, and the time t since the beginning of the experiment. Indeed since the target is under harsh conditions [16], the fissile material significantly evolves with time. Measurements of the ionic charge distribution and kinetic energy distribution of the same mass ($A = 136$) are regularly done throughout the whole experimental period in order to take into account this effect. This observable is called burn-up (BU). Finally, the relative mass yield $\mathcal{N}(A)$ is written

$$\mathcal{N}(A) = \sum_{E_k} \sum_{q} \frac{N(A, q, E_k, \Delta t_m, t)}{\mathrm{BU}(t) \times \Delta t_m \times E_k}, \tag{2}$$

where the division by E_k accounts for the energy acceptance ΔE_k which is proportional to E_k. Because of the limited beam time, it is impossible to thoroughly measure all E_k and q. Moreover, it has been shown that a correlation exists between E_k and q [18–20,22,23]. To take into account this effect, at least three measurements of the kinetic energy distribution are done at three different ionic charges $q_{i=1,...,3}$. Then, two linear fits are performed: one of the mean kinetic energy $\overline{E_k}$ as a function of the ionic charge and one of the standard deviation σ_{E_k} as a function of the ionic charge. Therefore, three estimations of the relative mass yield $\mathcal{N}(A, q_i)$ are computed. An additional ionic charge distribution measurement is performed, for a fixed kinetic energy $E_k^\times$. This measurement allows one to weight each kinetic energy distribution by the probability of production of the given ionic charge $P(q_i)$. Note that this distribution is corrected from the correlation between

E_k and q as explained previously. Finally, Eq. (2) becomes

$$\mathcal{N}(A, q_i) = \frac{1}{P(q_i)} \sum_{E_k} \frac{N(A, q_i, E_k, \Delta t_m, t)}{\mathrm{BU}(t) \times \Delta t_m \times E_k},$$

$$P(q) \propto N(A, q, E_k^\times, \Delta t_m, t) \exp\left(-\frac{(\overline{E_k}(q) - E_k^\times)^2}{2\sigma_{E_k}^2(q)}\right),$$

$$\sum_q P(q) = 1. \tag{3}$$

These relative mass yields are then combined to have one final estimation of the mass yield $\overline{\mathcal{N}}(A)$ by taking into account the covariance matrix $C_{ij} = \mathrm{Cov}(\mathcal{N}(A, q_i), \mathcal{N}(A, q_j))$. The dependences between the $\mathcal{N}(A, q_i)$ are held by $P(q)$ and $\mathrm{BU}(t)$. Therefore, $P(q)$ and $\mathrm{BU}(t)$ are used to build this covariance matrix as detailed in Refs [20,21]. $\overline{\mathcal{N}}(A)$ is written

$$\overline{\mathcal{N}}(A) = \left(\sum_{i,j} C_{ij}^{-1}\right)^{-1} \left(\sum_{i,j} C_{ij}^{-1} \mathcal{N}(A, q_j)\right). \tag{4}$$

Then a χ^2 test is performed with a confidence level of 90%. If it is unsuccessful, then an additional independent uncertainty is added to the diagonal elements of the covariance matrix C [20]. This additional uncertainty reflects the dispersion of the measurements and the limits of the procedure explained above. At the end, the absolute mass yield is

$$Y(A) = 2 \times \frac{\overline{\mathcal{N}}(A)}{\sum_A \overline{\mathcal{N}}(A)}. \tag{5}$$

However, it is difficult to measure all masses on the LOHENGRIN facility. Nevertheless, the collaboration aim is to provide absolute mass yields independently from nuclear databases. Therefore, at least 99.5% of a mass yield peak (heavy or light) is measured. The induced bias is taken into account in the final uncertainty for all measured masses. It should be noted that several campaigns are required to obtain enough experimental data. At least ten masses are common between each campaign. A cross normalization between each campaign is performed using these masses.

Here is a synthesis of how measurements and associated analysis of the mass yields are performed on the LOHENGRIN recoil spectrometer:

(1) Measurements of at least three kinetic energy distributions for different ionic charges q_i and one ionic charge distribution at $E_k^\times$ with the IC.
(2) Computation of the correlation between E_k and q through linear fits of $\overline{E_k}(q)$ and $\sigma_{E_k}(q)$.
(3) Computation of the relative mass yield for each kinetic energy distribution $\mathcal{N}(A, q_i)$ using Eq. (3).
(4) Computation of the average relative mass yield $\overline{\mathcal{N}}(A)$ using Eq. (4).
(5) Computation of the absolute mass yield using Eq. (5).

B. Isotopic yield

Assessment of nuclear charge of fission products is performed through the measurement of the associated β^- delayed γ emission. To detect these γ rays, two clovers are used at
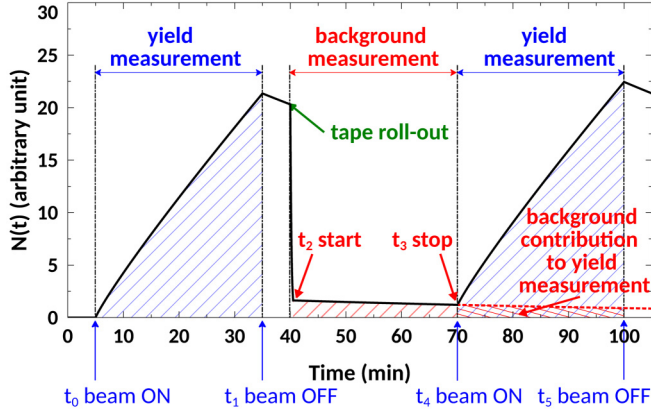
FIG. 1. Scheme of the isotopic evolution $N(t)$ over time. The full lines correspond to the deposited isotopes on the tape and on the vacuum chamber. When the tape is moved and the LOHENGRIN setting is changed, a background can be detected and must be subtracted. This background is coming from ions implanted into the window support grid and ions scattered to the vacuum chamber edges.

the "curved" position. Each clover is made of four HPGe detectors and surrounds a vacuum chamber with a movable tape inside. The beam associated to a specific triplet selection (A, q, E_k) is implanted on the movable tape. During the implantation (beam ON), the associated γ rays are recorded during a time range $\Delta t_m = 20$–30 minutes. Then, the tape is moved to remove the remaining radioactivity (beam OFF). A new measurement (beam OFF) of $\Delta t_m = 20$–30 minutes is started in order to estimate the background coming from the vacuum chamber. Indeed the beam is not perfectly collimated. Therefore, certain amount of ions are implanted on the vacuum chamber instead of the movable tape. After measuring the background, the LOHENGRIN setting is changed to a new triplet selection (A', q', E'_k) and a new collection is started (beam ON). Figure 1 sums up the method.

For a given mass, only the ionic charge distribution is measured with the γ detectors at a given kinetic energy $E_k^\times$, because of the limited beam time. The number of decays N_d of an isotope is written

$$N_{d_\gamma}(A, Z, q, E_k^\times, \Delta t_m, t) = \frac{N_\gamma(A, Z, q, E_k^\times, \Delta t_m, t)}{\epsilon_\gamma I_\gamma f_\gamma}. \quad (6)$$

The number of counts N_γ of a given γ transition is extracted using program Tv [24]. The efficiency ϵ_γ is extracted from a Monte Carlo simulation of the experimental setup. Then, it is validated using experimental data from point sources (^{60}Co, ^{133}Ba, ^{207}Bi) and online beam isotopes (^{96}Y, ^{134}Te), both covering the range 100 keV – 2.3 MeV. The intensity I_γ has been taken from a nuclear database [25]. I_γ is the product of a relative factor I_γ^{rel} and a normalization factor I_{norm}^γ: $I_\gamma = I_\gamma^{rel} I_{norm}^\gamma$. Finally, the sum effect correction factor f_γ is calculated with the TRUECOINC software [26]. This factor reflects the misestimation of the detected γ transition. Sometimes two successive γ rays (E_{γ_1}, E_{γ_2}) of the same cascade can be detected simultaneously as one γ transition

($E_\gamma = E_{\gamma_1} + E_{\gamma_2}$). At this step, the different γ rays are used to estimate an average number of decays, $\overline{N_d}$:

$$\overline{N_d}(A, Z, q, E_k^\times, \Delta t_m, t)$$
$$= \left(\sum_{i,j} C_{ij}^{-1}\right)^{-1} \left(\sum_{i,j} C_{ij}^{-1} N_{d_{\gamma_j}}(A, Z, q, E_k^\times, \Delta t_m, t)\right) \quad (7)$$

with $C_{ij} = \text{Cov}(N_{d_{\gamma_i}}, N_{d_{\gamma_j}})$. Details on the building of this matrix can be found in Ref. [20]. Similarly to the mass yield case, if the χ^2 test with a confidence level of 90% is unsuccessful, an additional uncertainty is taken into account. Only contributions coming from fission (and not from the deposited background) are of interest. Assessment of the number of decays coming from the contamination of the vacuum chamber $N_{d_{cont}}$ is detailed in the last section of Appendix A. Therefore the corrected number of decays coming from the nuclear fission process N_{d_f} is written

$$\overline{N_{d_f}}(A, Z, q, E_k^\times, \Delta t_m, t)$$
$$= \overline{N_d}(A, Z, q, E_k^\times, \Delta t_m, t)$$
$$- \overline{N_{d_{cont}}}(A, Z, q, E_k^\times, \Delta t_m, t). \quad (8)$$

The next step is to compute the fission rate τ by resolving the matrix form of the Bateman equations:

$$\boldsymbol{\tau}(A, q, E_k^\times, t) = \boldsymbol{B} \boldsymbol{N}_{d_f}(A, q, E_k^\times, \Delta t_m, t) \quad (9)$$

with $\boldsymbol{\tau}(A, q, E_k^\times, t)$ the vector of $\tau(A, Z, q, E_k^\times, t)$ and $\boldsymbol{N}_{d_f}(A, q, E_k^\times, \Delta t_m, t)$ the vector of $N_{d_f}(A, Z, q, E_k^\times, \Delta t_m, t)$. B [from Eq. (A11)] values depend on the branching ratios (from one isotope to another), the decay probability λ of each isotope of the isobaric chain, and the acquisition time Δt_m. See Appendix for more details on corrections involving Bateman equations.

Then, the fission rate is corrected by the probability of production of the given kinetic energy $P(E_k^\times)$ to assess the relative isotopic yield $\mathcal{N}(A, Z)$. However, this probability also depends on the ionic charge as previously explained. Therefore, this probability is expressed as

$$P(E_k^\times) = \int_{E_k^\times - \frac{\Delta E_k^\times}{2}}^{E_k^\times + \frac{\Delta E_k^\times}{2}} \rho(E_k) \, dE_k,$$
$$\rho(E_k) = \frac{1}{\sqrt{2\pi} \sigma_{E_k}(q)} \exp\left(-\frac{[E_k - \overline{E_k}(q)]^2}{2\sigma_{E_k}(q)^2}\right). \quad (10)$$

Quantities $\overline{E_k}(q)$ and $\sigma_{E_k}(q)$ are derived from the measurements of the (at least) three different kinetic energy distributions obtained with the IC. A linear evolution is expected for both quantities. This approach implies two approximations. First a Gaussian form of the kinetic energy distribution is supposed. Second, the probability $P(E_k)$ is supposed to be independent of the isotope. Indeed, the kinetic energy distribution measured with the IC is related to the mass (here

$A = 139$) and not the isotope. $\mathcal{N}(A, Z)$ is then written

$$\mathcal{N}(A, Z) = \sum_q \frac{\tau(A, Z, q, E_k^\times, t)}{\mathrm{BU}(t) \times P(E_k^\times)}. \tag{11}$$

The absolute normalization is achieved in two steps. First, the isobaric chain $A = 139$ is considered as a reference. Indeed, four isotopes, ^{139}I, ^{139}Xe, ^{139}Cs, and ^{139}Ba, are detected for this chain. The independent yield sum of these four isotopes corresponds approximately to 99.5% of the mass yield according to the nuclear data libraries [27,28]. The bias from the nonobserved 0.5% is taken into account in the final uncertainty similarly to the mass yield absolute normalization. This latter is negligible by comparison with the other sources of uncertainties. Then it can be written

$$Y(A = 139) = k_{139} \sum_Z \mathcal{N}(A = 139, Z). \tag{12}$$

Finally, the absolute isotopic yields can be written for all masses and isotopes:

$$Y(A, Z) = k_{139} \times \mathcal{N}(A, Z). \tag{13}$$

However, this solution is not optimal since the absolute isotopic yields of all the measured masses are dependent on the ones from mass 139. Unfortunately, this is the only solution to get absolute isotopic yields since not all nuclei for a given mass are detected (except for $A = 139$).

Below is a synthesis of how measurements and associated analysis of the isotopic yields are performed on the LOHENGRIN recoil spectrometer:

(1) Carrying out the same procedure as for the mass yield case.
(2) Measurement of the ionic charge distribution with HPGe clovers by implanting ions on a movable tape. Between each ionic charge measurement, a background measurement is performed (see Fig. 1).
(3) Extraction of the number of counts for each detected γ-rays using program Tv.
(4) Computation of the number of decays for each γ ray using Eq. (6).
(5) Computation of the average number of decays using Eq. (7).
(6) Correction of the background coming from the vacuum chamber using Eq. (8).
(7) Resolution of the Bateman equations to assess the fission rate τ using Eq. (9).
(8) Correction of the correlation between E_k and q using Eq. (10).
(9) Computation of the relative isotopic yield using Eq. (11).
(10) Computation of the absolute isotopic yield using Eqs. (12) and (13).

Figure 2 shows the absolute isotopic yields for the mass $A = 139$ with the associated covariance matrix for two cases. On the left is shown the case using the actual uncertainties of I_γ and on the right is shown the case using the uncertainty of the normalization intensity $I_{\mathrm{norm}}^\gamma = 0$. In the latter, the total uncertainty is reduced by a factor of 4. The covariance
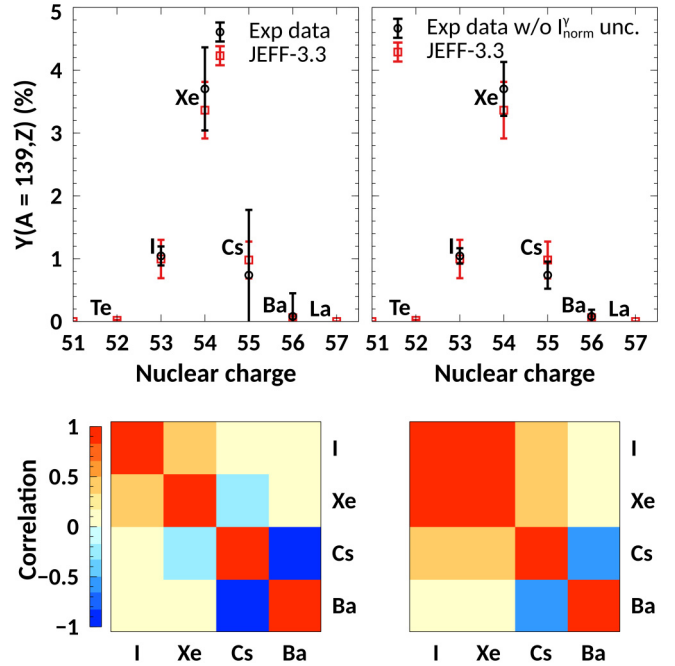
FIG. 2. Absolute isotopic yields for the mass $A = 139$ with all the uncertainties propagated (left) and for the case where $\Delta I_{\mathrm{norm}}^\gamma = 0$ (right). A comparison with the JEFF-3.3 library is also displayed. Correlation matrices in both cases are also displayed (bottom).

matrix is also modified. In other words, the uncertainties are mainly coming from nuclear decay data. By improving these data, more accurate isotopic yields can be extracted. Finally, a comparison with the JEFF-3.3 database is also displayed and shows an overall good agreement. The experimental data were recorded in May 2013 [29] using a 7×0.5 cm^2 target of 282 μg cm^{-2} of ^{241}Pu covered by a thin nickel foil (≈ 0.25 μm). This campaign was designed to measure isotopic yields for 8 masses. The derived local odd-even effect is $\delta_Z(A = 139) = 0.36 \pm 0.32$ in comparison with JEFF-3.3, $\delta_Z^{\mathrm{JEFF-3.3}}(A = 139) = 0.27 \pm 0.12$.

IV. FROM LOCAL ODD-EVEN EFFECT TO NEUTRON EMISSION USING FIFRELIN

In this work, the local odd-even effect $\delta_Z(A)$ as a function of the fission product kinetic energy for the mass $A = 139$ is computed. An experimental campaign in July 2016 [30] was carried out with a thinner target (208 μg cm^{-2} of ^{241}Pu on 7×0.5 cm^2) still covered by a thin nickel foil (≈ 0.25 μm). Here, all the steps described before are not necessary to extract the isotopic yields. For instance, it is counterproductive to correct $P(E_k)$, since an evolution of the fission product kinetic energy is investigated. The absolute normalization is also not necessary.

To interpret these results, a comparison with the Monte Carlo code FIFRELIN is performed. The aim is to test FIFRELIN assumptions. If an agreement is reached between the experimental data and FIFRELIN calculations, we can get feedback from the models used by FIFRELIN (the temperature ratio law for instance). However, energy loss corrections are needed to

go from the calculations (which directly reflect the fission process) to the experimental data. In the following part, details on the input data and the models used by FIFRELIN are presented. The energy loss correction process is also described. Finally, a sensitivity study on the main ingredients of the simulation will be shown.

A. FIFRELIN

FIssion Fragment Evaporation Leading to an Investigation of Nuclear data (FIFRELIN) [31–33] is a Monte Carlo code developed at CEA Cadarache since 2010. Initially, the aim was to describe the deexcitation of fission fragments from their formation (after being fully accelerated) until they reach their ground state or a metastable state which then decay through β decay. Nowadays, the code can theoretically describe the deexcitation of any nucleus starting from a given nuclear level. FIFRELIN relies on preneutron nuclear data and models to compute the most accurate deexcitation path. The code can be split into two parts.

First, the fission process creates two fission fragments with a given mass, nuclear charge, kinetic energy, excitation energy, spin, and parity. Note that no complete set of experimental data exists for the reaction ^{241}Pu (n_{th}, f). Therefore, the preneutron isotopic yields $Y(A, Z)$ and total kinetic energy (TKE) yields $Y(\mathrm{TKE}, A)$ are coming from the GEF code [34]. FIFRELIN samples the light fission fragment mass and nuclear charge using the $Y(A, Z)$ distribution. The total kinetic energy is then sampled using the $Y(\mathrm{TKE}, A)$ distribution. The conservation laws allow one to assess the complementary heavy fragment characteristics (A, Z) and the associated kinetic energies (of both fragments). The repartition of the total excitation energy is mainly driven by a phenomenological temperature ratio law $R_{\mathrm{T}}(A)$ with two free parameters $\mathrm{RT}_{\min}$ and $\mathrm{RT}_{\max}$. By definition, there are three anchor points in the (A, R_{T}) space:

$$R_{\mathrm{T}}(A_{\mathrm{CN}}/2) = 1, \quad R_{\mathrm{T}}(A_{CN} - 78) = \mathrm{RT}_{\min}, \quad R_{\mathrm{T}}(132) = \mathrm{RT}_{\max}$$

with CN the compound nucleus. A linear interpolation is then made between each point. Finally the spin of each fission fragment is sampled from

$$P(J) \propto (2J + 1)\exp\left(-\frac{(J + 1/2)^2}{2\sigma^2}\right) \qquad (14)$$

with σ^2 a free parameter for each fission fragment mass region (light and heavy). Those four free parameters are set using a target observable. Here, the target observable is the total average prompt neutron multiplicity $\overline{\nu} = 2.92$ [28]. The four parameters which reproduce this value are $\mathrm{RT}_{\min} = 0.5$, $\mathrm{RT}_{\max} = 1.2$, $\sigma_L = 7.2\hbar$, and $\sigma_H = 8.6\hbar$.

Second, both fission fragments will emit prompt (n, γ, e^-) particles until they reach a β decaying state. To do so, FIFRELIN completes the experimental nuclear level schemes coming from RIPL-3 database [35,36] by using nuclear level density (here the composite Gilbert and Cameron model [37]) and spin models (here the back-shifted Fermi gas model [35,36]). Once the nuclear nuclear level scheme is complete, the probability to go from a nuclear level i to a nuclear level j by emitting either n, γ, or e^- is

calculated within the notion of nuclear realization [33,38]. In this framework, different nuclear level schemes (for a given isotope) can be sampled, and for each sampled nuclear level scheme different deexcitation paths can be computed. For each emitted particle, different ingredients are used. The probabilities associated to the prompt neutron emission are calculated thanks to neutron transmission coefficients derived from an optical model (here the Koning-Delaroche model [39]). This optical model is used through the ECIS code [40]. The probabilities associated with the prompt γ emission are derived from the γ strength function (here, the enhanced generalized Lorentzian [41] model) and experimental information. The probabilities associated to the prompt e^- emission are calculated with the BRICC code [42] or come from experimental data.

FIFRELIN can compute the isotopic yields as a function of the fission product kinetic energy through an event-by-event analysis. However, the kinetic energy (after prompt neutron emission) computed by FIFRELIN needs to be corrected for the energy loss of fission products inside the target and its cover. To take it into account, FIFRELIN kinetic energy distributions are convoluted by a Landau distribution [43] which models the energy loss of ions through a thin layer [20,44]. Two free parameters are adjusted in order to reproduce the experimental kinetic energy distributions. Here, the energy loss is considered to be identical for each isotope of a given mass. Also, the parameters are adjusted for each BU point since the target and cover thickness may evolve over time (self-sputtering, oxidation of Ni foil, diffusion into backing [16]), Therefore, the mass $A = 136$ is used to fix the free parameters (see top plot in Fig. 3). Then, these fixed parameters are used to correct the kinetic energy distributions for $A = 139$ (see bottom plot in Fig. 3).

The comparison of experimental data and FIFRELIN of the local odd-even effect is shown in Fig. 4. The experimental point from the May 2013 campaign was added in order to show the reproducibility of the local odd-even effect using the LOHENGRIN spectrometer. In the following, only experimental data from July 2016 will be presented. Although FIFRELIN seems to overestimate the local odd-even effect, the same trend as in the experimental data can be observed. Finally, it is difficult to conclude on the agreement between FIFRELIN and the experimental data due to the large experimental uncertainties.

Therefore, a more precise and discriminant observable is needed to better estimate the difference between FIFRELIN calculations and the experimental data. The relative isotopic cumulative yields $\mathcal{N}_c$ integrated over a period of time of $\Delta t_m = 30$ minutes fit these specifications:

$$\mathcal{N}_c(A, Z, E_k^\times, \Delta t_m) = \sum_q \frac{N_d(A, q, E_k^\times, \Delta t_m, t)}{\mathrm{BU}(t)},$$

$$P_c(A, Z, E_k^\times, \Delta t_m) = \frac{\mathcal{N}_c(A, Z, E_k^\times, \Delta t_m)}{\sum_Z \mathcal{N}_c(A, Z, E_k^\times, \Delta t_m)}, \qquad (15)$$

with P_c the relative isotopic cumulative yield probability. To compare simulations with P_c, the Bateman equation resolution $\boldsymbol{B}^{-1}$ is applied to simulated data. Figure 5 shows the

Report_SANDA_Deliverable_D2.12_Julien-Laferriere_2020a
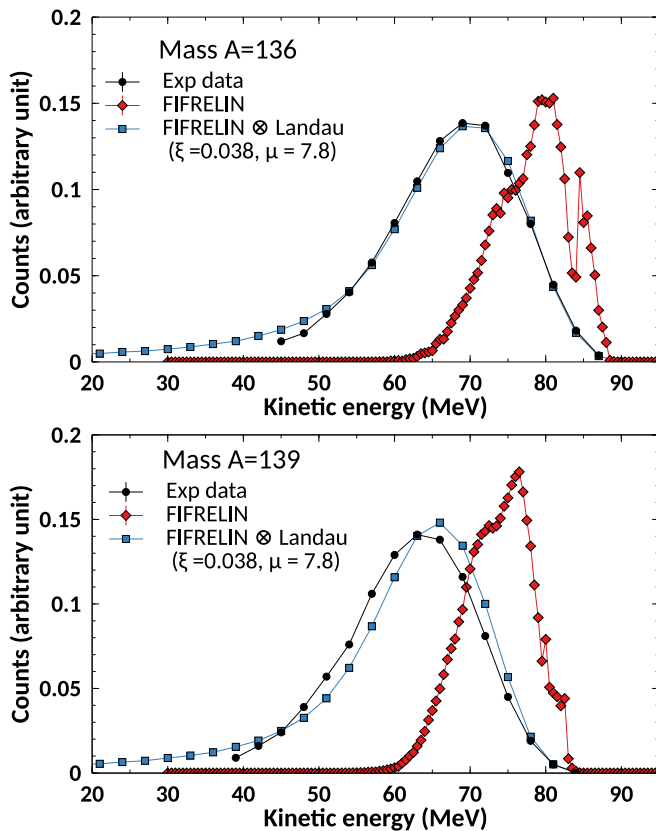
FIG. 3. Comparison between experimental kinetic energy distribution (black circle) and FIFRELIN calculation (red points). An agreement is reached by convoluting FIFRELIN with the Landau distribution. Parameters were fixed thanks to the mass $A = 136$ (top) and applied to mass $A = 139$ (bottom). The lines are to guide the eye. The experimental kinetic energy refers to the LOHENGRIN selected energy, i.e., after the cover foil.
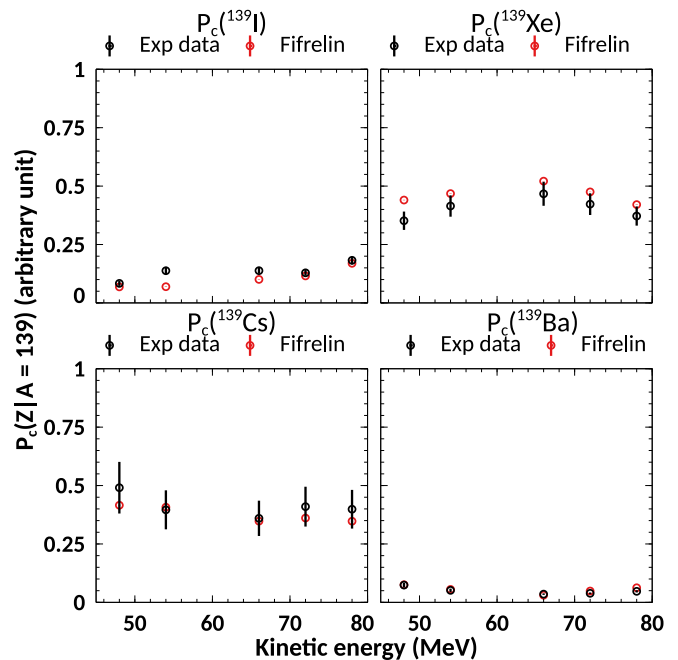
FIG. 5. Relative cumulated isotopic yield probability for experimental data (black points) and FIFRELIN calculations after energy loss corrections (red points). The experimental kinetic energy refers to the LOHENGRIN selected energy, i.e., after the cover foil.

results of such a comparison. The agreement between the experimental data and FIFRELIN is satisfactory even if a slight overestimation of FIFRELIN for Xe is observed. Indeed, all the experimental data (except the 54 MeV point for I) are compatible with FIFRELIN with a confidence level of 90%. In other words, FIFRELIN is validated in regards to the kinetic energy dependence of the mass $A = 139$.

B. Test of the model assumption

The next step is to look at the local odd-even effect as a function of the fission product kinetic energy computed by FIFRELIN without any energy loss correction. Figure 6 shows $\delta_Z(A)$ as a function of the fission product kinetic energy (top) and the excitation energy (before neutron emission) (bottom). The different color points represent the $\delta_Z(A)$ for fission events with different emitted neutrons. The results show that the structure of the $\delta_Z(A)$ depends on the number of emitted neutrons.

It must be reminded that the adjusted parameters of FIFRELIN were fixed according to the average total prompt neutron emission $\bar{\nu}$ and not by using the relative cumulative yields of the mass $A = 139$. Therefore, the predictive power of FIFRELIN can be tested with these new experimental data. The good agreement between FIFRELIN and the experimental data indicates that the underlying hypotheses used in FIFRELIN are satisfactory. According to Fig. 6, $\delta_Z(A)$ is driven by the neutron emission process. The neutron emission probability as a function of the excitation energy shows a steplike function, which can be interpreted as the average neutron energy separation to emit 1, 2, . . . neutrons. In FIFRELIN, this process

FIG. 4. Comparison between experimental data from the July 2016 campaign (black points) and from the May 2013 campaign (green point) and FIFRELIN calculations with (blue curve) and without (red curve) energy loss corrections. The experimental kinetic energy refers to the LOHENGRIN selected energy, i.e., after the cover foil.
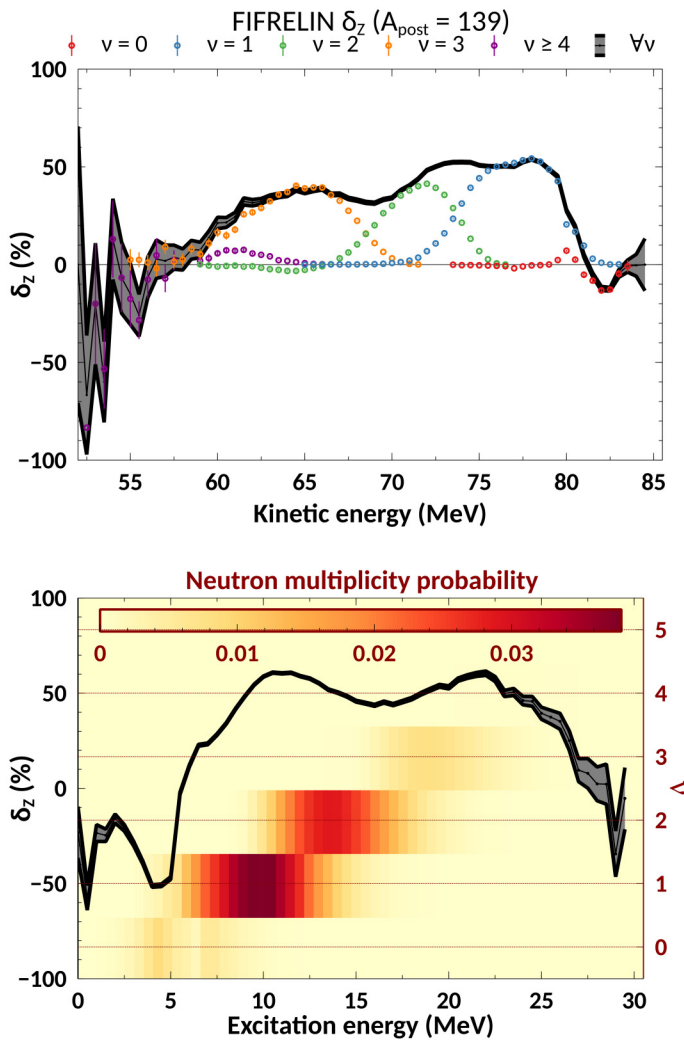
FIG. 6. Top: Local odd-even effect as a function of the fission product kinetic energy for different numbers of emitted neutrons: 0, 1, 2, 3, and $\geqslant 4$ (displayed in colors). Bottom: Local odd-even effect as a function of the excitation energy before neutron emission (y axis on the left). Local odd-even effect as a function of the number of emitted neutrons (y axis on the right). The associated probabilities are displayed in colors (z axis on the top). No energy loss correction is taken into account.

FIG. 7. Top: Local odd-even effect compared with the reference FIFRELIN calculation after a 0.1 shift on the parameter RT_{min} (with $RT_{min}^{ref} = 0.5$). A slight difference can be seen at higher kinetic energy. Bottom: Relative cumulated isotopic yield probability compared with the reference FIFRELIN calculation. No significant difference is observed (bottom). All calculations are corrected from the energy loss through the target and the cover foil.

is mainly due to the temperature ratio law and the neutron transmission coefficients.

A sensitivity analysis can be applied to two main ingredients of this analysis. The first one is the total excitation energy, which can be assessed through the temperature ratio law. To test the influence of the excitation energy on the local odd-even effect, a shift of ± 0.1 on the parameter RT_{min} (which corresponds to a shift of ± 2 MeV in excitation energy) is performed. Figure 7 shows the impact of such a shift on the local odd-even effect and on the relative cumulative isotopic yield probability. Relative quantities (to the reference FIFRELIN calculation) are plotted. It shows that the temperature ratio law modification changes the parity at higher kinetic energy only. Nevertheless, the measurements are not accurate enough to provide a new constraint on this temperature ratio law. It

can be explained by the impact of the energy loss through the target. With a thinner target, it should be possible to enhance the differences between the previous cases. Nonetheless, these results give confidence in the models and the processes used by FIFRELIN.

The second important ingredient is the preneutron isotopic yields. The aim is to test the reliability of these yields coming from GEF. To do so, the mean nuclear charge is shifted by ± 1 unit. In these cases, simulations are not in agreement with the experimental data anymore, as shown in Fig. 8. Therefore, the experimental data can also be used to validate the preneutron isotopic yields.

In conclusion, the experimental data can be seen as a local test for the mean neutron emission and the associated neutron probabilities within a restricted preneutron mass region (here $A = 139\text{--}143$).
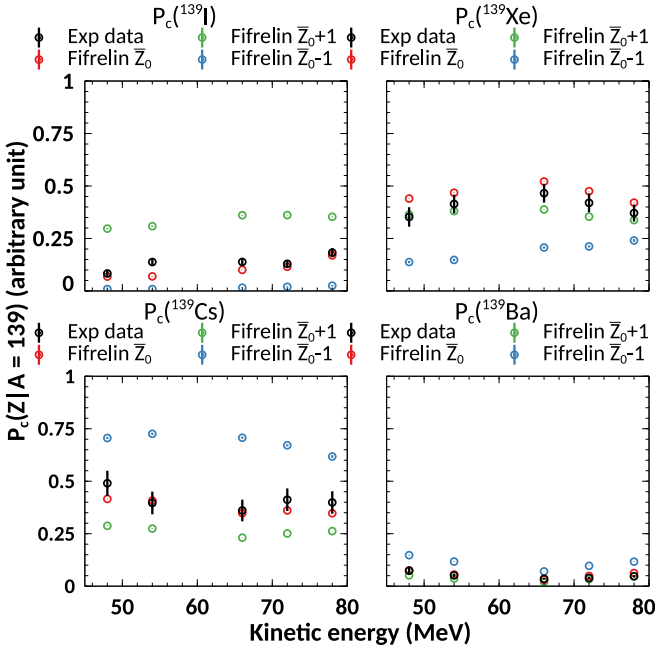
FIG. 8. Impact of one unit shift of the preneutron mean nuclear charge for all masses. A large impact is observed. The experimental kinetic energy refers to the LOHENGRIN selected energy, i.e., after the cover foil and the calculations are corrected from the energy loss through the target and the cover foil.

V. CONCLUSION AND OUTLOOK

The complete data analysis was presented and illustrated for the specific case of isobaric chain $A = 139$. Then, the local odd-even effect $\delta_Z(A)$ as a function of the fission product kinetic energy was assessed through measurements using the LOHENGRIN recoil spectrometer. Comparisons with the Monte Carlo code FIFRELIN were performed in order to interpret these experimental data in regards to the neutron emission process. The good match between the experimental results and the calculations coming from FIFRELIN indicates that the underlying models used are well chosen in the case of a fission event involving the mass $A = 139$. A sensitivity analysis shows these measurements are a probe to the local prompt neutron emission through all the deexcitation path assumptions used in FIFRELIN. However, the experimental data are not discriminant enough to highlight the impact of the initial excitation energy because of the energy loss inside the target. New measurements on a specific mass region (around $A = 132$) may give more constraints on the initial excitation energy and the temperature ratio law. These studies are complementary to the studies of the isomeric ratios evolution as a function of the fission product kinetic energy [11] or the studies of the correlation between the prompt γ cascade in coincidence with fission fragment and neutron observables [45–47].

ACKNOWLEDGMENTS

APPENDIX A: RESOLUTION OF BATEMAN EQUATIONS

In this Appendix, we detail the way to go from the number of decays N_d of an isotope to the fission rate τ.

1. With a source term τ

The activities of a decay chain are ruled by the Bateman equation:

$$\frac{dN_0(t)}{dt} = -\lambda_0 N_0(t) + \tau_0,$$
$$\frac{dN_1(t)}{dt} = -\lambda_1 N_1(t) + \tau_1 + \mathrm{BR}_{0\to1}\lambda_0 N_0(t),$$
$$\vdots$$
$$\frac{dN_n(t)}{dt} = -\lambda_n N_n(t) + \tau_n + \sum_{i=0}^{n-1} \mathrm{BR}_{i\to n}\lambda_i N_i(t), \quad (A1)$$

with $N_{i=0,n}$ the population of the ith nucleus, $\lambda_{i=0,n}$ its decay probability, $\tau_{i=0,n}$ the associated fission source term and $\mathrm{BR}_{i\to j}$ the probability of decaying from the nucleus i to the nucleus j. This equation can be written in a matrix form:

$$\frac{dN(t)}{dt} = BLN(t) + T = AN(t) + T \quad (A2)$$

with

$$N = \begin{bmatrix} N_0 \\ \vdots \\ N_n \end{bmatrix}, \quad T = \begin{bmatrix} \tau_0 \\ \vdots \\ \tau_n \end{bmatrix}, \quad L = \begin{bmatrix} \lambda_0 & & 0 \\ & \ddots & \\ 0 & & \lambda_n \end{bmatrix},$$

$$B = \begin{bmatrix} -1 & & 0 \\ & \ddots & \\ \mathrm{BR}_{i\to j} & & -1 \end{bmatrix}.$$

For each isotope i of the decay chain, the detected γ transition N_i^γ, during the measuring time Δt_m is written

$$\forall i, \; N_i^\gamma(\Delta t_m) = I_\gamma \epsilon_\gamma f_\gamma \int_0^{\Delta t_m} \lambda_i N_i(t)dt$$

$$\Leftrightarrow \frac{N_i^\gamma}{I_\gamma \epsilon_\gamma f_\gamma} = \int_0^{\Delta t_m} \lambda_i N_i(t)dt = N_{d_i}(\Delta t_m) \quad (A3)$$

with I_γ, ϵ_γ, and f_γ the intensity, the detection efficiency and the sum effect correction factor respectively. If we define

$$\forall i, \; X_i(\Delta t_m) = \int_0^{\Delta t_m} N_i(t)dt, \quad (A4)$$

then

$$N_d(t) = LX(t) \quad (A5)$$

Since the functions used are $\mathcal{C}^1$ class, we can integrate and switch the derivative and the integration of Eq. (A2):

$$\frac{dX(t)}{dt} = AX(t) + tT. \quad (A6)$$

To make $N_d(t)$ appear, we need to multiply Eq. (A6) by $\boldsymbol{L}$ and define $\boldsymbol{S} = \boldsymbol{L}\boldsymbol{A}\boldsymbol{L}^{-1}$:

$$\frac{dN_d(t)}{dt} = \boldsymbol{S}N_d(t) + t\boldsymbol{L}\boldsymbol{T}. \qquad (A7)$$

Here $\boldsymbol{S}$ is an inferior triangle matrix; we can then diagonalize it: $\boldsymbol{S} = \boldsymbol{R}\boldsymbol{D}\boldsymbol{R}^{-1}$. If we define $\boldsymbol{Y}(t) = \boldsymbol{R}^{-1}N_d(t)$ and $\boldsymbol{C} = \boldsymbol{R}^{-1}\boldsymbol{L}\boldsymbol{T}$ and multiply Eq. (A7) by $\boldsymbol{R}^{-1}$, it reads

$$\frac{d\boldsymbol{Y}(t)}{dt} = \boldsymbol{D}\boldsymbol{Y}(t) + t\boldsymbol{C}. \qquad (A8)$$

Since $\boldsymbol{D}$ is diagonal, we have n equations:

$$\forall i, \ \frac{dY_i(t)}{dt} = D_{ii}Y_i(t) + tC_i. \qquad (A9)$$

This is simply a first-order differential equation with time dependent tC_i second member. With the bounding condition $Y_i(t=0) = 0$ (which means that there was no nucleus at time 0), C_i is written

$$\forall i, \ C_i = \frac{D_{ii}^2}{e^{D_{ii}t} - 1 - D_{ii}t}Y_i(t) = E_{ii}(t)Y_i(t). \qquad (A10)$$

Finally,

$$\boldsymbol{T} = \boldsymbol{B}N_d(t) \quad \text{with} \quad \boldsymbol{B} = \boldsymbol{L}^{-1}\boldsymbol{R}\boldsymbol{E}(t)\boldsymbol{R}^{-1}$$

and the diagonal matrix $\boldsymbol{E}(t) = \dfrac{\boldsymbol{D}^2}{e^{\boldsymbol{D}t} - 1 - \boldsymbol{D}t}$. (A11)

2. Without a source term

Moreover, in the case of the background correction, the Bateman equation to resolve is

$$\frac{dN(t)}{dt} = \boldsymbol{A}N(t) \qquad (A12)$$

When integrating within a time t, we have

$$\frac{d\boldsymbol{X}(t)}{dt} = \boldsymbol{A}\boldsymbol{X}(t) + \boldsymbol{M} \Leftrightarrow \frac{dN_d(t)}{dt} = \boldsymbol{S}N_d(t) + \boldsymbol{L}\boldsymbol{M} \quad (A13)$$

with $\boldsymbol{M}$ the unknown which is related to the initial number of the nucleus. At the end, we have

$$\boldsymbol{M} = \boldsymbol{B}N_d(t) \quad \text{with} \quad \boldsymbol{B} = \boldsymbol{L}^{-1}\boldsymbol{R}\boldsymbol{E}(t)\boldsymbol{R}^{-1}$$

and the diagonal matrix $\boldsymbol{E}(t) = \dfrac{\boldsymbol{D}}{e^{\boldsymbol{D}t} - 1}$. (A14)

3. Analysis method and background correction

For the background correction, an additional step must be performed in order to assess the parameter $N_{d_{\mathrm{cont}}}$ which reflects the contribution of vacuum residual background on a new measurement. Figure 1 shows the origin of the background. In the time interval $t = [t_0, t_1]$ the background coming from the vacuum chamber is recorded, $N_{d_{\mathrm{bkg}}}(t_1)$, and it allows one to determine $\boldsymbol{M}$. We suppose that there is no initial background $[N_d(t=t_0) = 0]$, then $N_{d_{\mathrm{bkg}}}(t=t_0) = 0$:

$$N_{d_{\mathrm{bkg}}}(t_1) = \frac{N_i^\gamma(t_1)}{I_\gamma \epsilon_\gamma f_\gamma}. \qquad (A15)$$

The contribution from the background during the measurement in the time interval $t = [t_2, t_3]$ is

$$N_{d_{\mathrm{cont}}} = \int_{t_2}^{t_3} \boldsymbol{L}N(t)dt = N_d(t_3) - N_d(t_2). \qquad (A16)$$

From Eqs. (A5) and (A14), Eq. (A16) is written

$$N_{d_{\mathrm{cont}}} = [\boldsymbol{B}^{-1}(t_3) - \boldsymbol{B}^{-1}(t_2)]\boldsymbol{M},$$
$$N_{d_{\mathrm{cont}}} = [\boldsymbol{B}^{-1}(t_3) - \boldsymbol{B}^{-1}(t_2)]\boldsymbol{B}(t_1)N_{d_{\mathrm{bkg}}}(t_1),$$
$$N_{d_{\mathrm{cont}}} = \boldsymbol{R}[\boldsymbol{E}^{-1}(t_3) - \boldsymbol{E}^{-1}(t_2)]\boldsymbol{E}(t_1)\boldsymbol{R}^{-1}N_{d_{\mathrm{bkg}}}(t_1)$$
$$\Leftrightarrow N_{d_{\mathrm{cont}}} = \boldsymbol{R}\left(\frac{e^{\boldsymbol{D}t_3} - e^{\boldsymbol{D}t_2}}{e^{\boldsymbol{D}t_1} - 1}\right)\boldsymbol{R}^{-1}N_{d_{\mathrm{bkg}}}(t_1). \qquad (A17)$$

APPENDIX B: GLOSSARY

This section summarizes all the notations used in the analysis part of the article.

A: mass of the nucleus $^A_Z\mathrm{X}$

Z: nuclear charge of the nucleus $^A_Z\mathrm{X}$

$\delta_Z(A)$: local odd-even effect

q: ionic charge

q_i: ionic charge for which kinetic energy distributions are performed

E_k: kinetic energy

ΔE_k: kinetic energy resolution

$E_k^\times$: kinetic energy for which ionic charge distributions are performed

$\overline{E_k}$: mean kinetic energy extracted from the kinetic energy distribution

σ_{E_k}: standard deviation extracted from the kinetic energy distribution

t: time when the measurement is made since the beginning of the experimental campaign

Δt_m: measuring time

BU(t) (burn-up): constructed observable in order to follow the loss of fissile material from the target as a function of time

$N(A, q, E_k, \Delta t_m, t)$: number of counts extracted from the ionization chamber

$\mathcal{N}(A, q_i)$: relative mass yield calculated from the kinetic energy distribution measured with the ionic charge q_i

$P(q)$: ionic charge probability derived from the ionic charge distribution

$\mathrm{Cov}(\mathcal{N}(A, q_i), \mathcal{N}(A, q_j))$: element of the covariance matrix between the relative mass yield calculated from the kinetic energy distributions measured at q_i and q_j

$\overline{\mathcal{N}}(A)$: average relative mass yield

$Y(A)$: absolute mass yield

ϵ_γ: detection efficiency for a given γ transition

I_γ: absolute intensity for a given γ transition

I_γ^{rel}: relative intensity for a given γ transition

I_{norm}^γ: normalization factor for γ intensity

f_γ: sum effect correction factor for a given γ transition

$N_\gamma(A, Z, q, E_k^\times, \Delta t_m, t)$: number of counts extracted from the γ detectors for a given γ transition

Report_SANDA_Deliverable_D2.12_Julien-Laferriere_2020a

$N_{d_\gamma}(A, Z, q, E_k^\times, \Delta t_m, t)$: number of decays derived from a given γ transition

$\overline{N_d}(A, Z, q, E_k^\times, \Delta t_m, t)$: average number of decays

$\text{Cov}(N_{d_{\gamma_i}}, N_{d_{\gamma_j}})$: element of the covariance matrix between the number of decays derived from the γ transition γ_i and the gamma transition γ_j

$\overline{N_{d_{\text{bkg}}}}(A, Z, q, E_k^\times, \Delta t_m, t)$: average number of decays measured during the background measurement

$\overline{N_{d_{\text{cont}}}}(A, Z, q, E_k^\times, \Delta t_m, t)$: average number of decays contaminating the current measurement

$\overline{N_{d_f}}(A, Z, q, E_k^\times, \Delta t_m, t)$: average corrected number of decays

$\boldsymbol{B}$: matrix related to the Bateman equation resolution

$\tau(A, Z, q, E_k^\times, t)$: fission rate

$P(E_k^\times)$: probability to have the fission product at the selected kinetic energy $E_k^\times$

$\mathcal{N}(A, Z)$: relative independent isotopic yield

$\mathcal{N}_c(A, Z, E_k^\times, \Delta t_m)$: relative cumulative isotopic yield for a given kinetic energy

$P_c(A, Z, E_k^\times, \Delta t_m)$: relative cumulative isotopic yield probability for a given kinetic energy

k_{139}: normalization factor linking relative to absolute isotopic yield using the mass $A = 139$

$Y(A, Z)$: absolute isotopic yield

---

[1] O. Hahn and F. Strassmann, Naturwissenschaften **27**, 11 (1939).

[2] L. Meitner and O. R. Frisch, Nature (London) **143**, 239 (1939).

[3] H. Goutte, J. F. Berger, P. Casoli, and D. Gogny, Phys. Rev. C **71**, 024316 (2005).

[4] P. Möller, A. J. Sierk, and A. Iwamoto, Phys. Rev. Lett. **92**, 072501 (2004).

[5] J. Randrup and P. Möller, Phys. Rev. Lett. **106**, 132503 (2011).

[6] E. Torleif, Adv. Phys. **9**, 425 (1960).

[7] P. Fong, Phys. Rev. **102**, 434 (1956).

[8] B. D. Wilkins, E. P. Steinberg, and R. R. Chasman, Phys. Rev. C **14**, 1832 (1976).

[9] J. R. Nix and W. J. Swiatecki, Nucl. Phys. **71**, 1 (1965).

[10] Y. Aritomo, S. Chiba, and F. Ivanyuk, Phys. Rev. C **90**, 054609 (2014).

[11] A. Chebboubi, G. Kessedjian, O. Litaize, O. Serot, H. Faust, D. Bernard, A. Blanc, U. Köster, O. Méplan, P. Mutti, and C. Sage, Phys. Lett. B **775**, 190 (2017).

[12] J. Kaufmann, W. Mollenkopf, F. Gönnenwein, P. Geltenbort, and A. Oed, Z. Phys. A **341**, 319 (1992).

[13] U. Quade, K. Rudolph, S. Skorka, P. Armbruster, H.-G. Clerc, W. Lang, M. Mutterer, C. Schmitt, J. Theobald, F. Gönnenwein, J. Pannicke, H. Schrader, G. Siegert, and D. Engelhardt, Nucl. Phys. A **487**, 1 (1988).

[14] N. Boucheneb, P. Geltenbort, M. Asghar, G. Barreau, T. Doan, F. Gönnenwein, B. Leroux, A. Oed, and A. Sicre, Nucl. Phys. A **502**, 261 (1989).

[15] P. Armbruster, M. Asghar, J. P. Bocquet, R. Decker, H. Ewald, J. Greif, E. Moll, B. Pfeiffer, H. Schrader, F. Schussler, G. Siegert, and H. Wollnik, Nucl. Instrum. Methods **139**, 213 (1976).

[16] U. Köster, H. Faust, T. Materna, and L. Mathieu, Nucl. Instrum. Methods A **613**, 363 (2010).

[17] G. Fioni, H. R. Faust, M. Gross, M. Hesse, P. Armbruster, F. Gönnenwein, and G. Münzenberg, Nucl. Instrum. Methods A **332**, 175 (1993).

[18] F. Martin, Etude des distributions en masse, charge nucléaire et énergie cinétique des produits de fission de l'233U(nth,f) et du 241Pu(nth,f) mesurées auprès du spectromètre de masse Lohengrin (ILL), Ph.D. thesis, Université de Grenoble, 2013, https://tel.archives-ouvertes.fr/tel-01288258/document.

[19] A. Chebboubi, Contribution à l'étude de la fission nucléaire: de LOHENGRIN à FIPPS, Ph.D. thesis, Université Grenoble Alpes, 2015, https://tel.archives-ouvertes.fr/tel-01272599/document.

[20] S. Julien-Laferrière, Approche expérimentale et phénoménologique des rendements de la fission induite par neutron thermique du 239Pu et du 241Pu, Ph.D. thesis, Université Grenoble Alpes, 2018, https://tel.archives-ouvertes.fr/tel-01995046/document.

[21] S. Julien-Laferrière, A. Chebboubi, G. Kessedjian, and O. Serot, EPJ Nucl. Sci. Technol. **4**, 25 (2018).

[22] Y. K. Gupta, D. C. Biswas, O. Serot, D. Bernard, O. Litaize, S. Julien-Laferrière, A. Chebboubi, G. Kessedjian, C. Sage, A. Blanc, H. Faust, U. Köster, A. Ebran, L. Mathieu, A. Letourneau, T. Materna, and S. Panebianco, Phys. Rev. C **96**, 014608 (2017).

[23] A. Chebboubi, S. Julien-Laferrière, J. Nicholson, G. Kessedjian, O. Serot, A. Blanc, D. Bernard, H. Faust, Y. Kim, U. Köster, A. Letourneau, O. Litaize, O. Méplan, P. Mutti, M. Rapala, M. Ramdhane, and C. Sage, EPJ Web Conf. (to be published).

[24] J. Theuerkauf, S. Esser, S. Krink, M. Luig, N. Nicolay, O. Stuch, and H. Wolters, *Program Tv* (Institute for Nuclear Physics, Cologne, 1993).

[25] Y. Khazov, A. A. Rodionov, S. Sakharov, and B. Singh, Nucl. Data Sheets **104**, 497 (2005).

[26] S. Sudár, TrueCoinc - A program for calculation of true co-incidence correction for gamma rays, Tech. Rep. No. IAEA-TECDOC-1275 (Institute of Experimental Physics, Debrecen, 2009), pp. 37–48.

[27] M. Chadwick, M. Herman, P. Obložinský, M. Dunn, Y. Danon, A. Kahler, D. Smith, B. Pritychenko, G. Arbanas, R. Arcilla, R. Brewer, D. Brown, R. Capote, A. Carlson, Y. Cho, H. Derrien, K. Guber, G. Hale, S. Hoblit, S. Holloway, T. Johnson, T. Kawano, B. Kiedrowski, H. Kim, S. Kunieda, N. Larson, L. Leal, J. Lestone, R. Little, E. McCutchan, R. MacFarlane, M. MacInnes, C. Mattoon, R. McKnight, S. Mughabghab, G. Nobre, G. Palmiotti, A. Palumbo, M. Pigni, V. Pronyaev, R. Sayer, A. Sonzogni, N. Summers, P. Talou, I. Thompson, A. Trkov, R. Vogt, S. van der Marck, A. Wallner, M. White, D. Wiarda, and P. Young, Nucl. Data Sheets **112**, 2887 (2011).

[28] A. Santamarina, D. Bernard, P. Blaise, M. Coste, A. Courcelle, T. Huynh, C. Jouanne, P. Leconte, O. Litaize, S. Mengelle, G. Noguère, J.-M. Ruggiéri, O. Serot, J. Tommasi, C. Vaglio, and J.-F. Vidal, The JEFF-3.1.1 Nuclear Data Library, Tech. JEFF Rep. No. 22 (NEA, Paris, 2009).

[29] O. Serot, D. Bernard, S. Chabod, A. Chebboubi, H. Faust, G. Kessedjian, U. Köster, A. Letourneau, O. Litaize, F. Martin, T. Materna, O. Méplan, S. Panebianco, and C. Sage, Fission

Report_SANDA_Deliverable_D2.12_Julien-Laferriere_2020a

product yield measurements in the heavy mass region for the 241pu(nth,f) reaction, Institut Laue-Langevin (ILL) dataset, doi: 10.5291/ILL-DATA.3-01-596 (2013).

[30] O. Litaize, C. Amouroux, D. Bernard, A. Blanc, A. Chebboubi, H. Faust, G. Kessedjian, U. Köster, A. Letourneau, T. Materna, O. Méplan, S. Panebianco, C. Sage, and O. Serot, Isotopic and isomeric yields measurement in the near symmetric mass region of the 241pu(nth,f) reaction, Institut Laue-Langevin (ILL) dataset, doi: 10.5291/ILL-DATA.3-01-624 (2016).

[31] O. Litaize and O. Serot, Phys. Rev. C **82**, 054616 (2010).

[32] O. Litaize, O. Serot, and L. Berge, Eur. Phys. J. A **51**, 177 (2015).

[33] D. Regnier, O. Litaize, and O. Serot, Comput. Phys. Commun. **201**, 19 (2016).

[34] K.-H. Schmidt, B. Jurado, C. Amouroux, and C. Schmitt, Nucl. Data Sheets **131**, 107 (2016).

[35] R. Capote, M. Herman, P. Obložinský, P. Young, S. Goriely, T. Belgya, A. Ignatyuk, A. Koning, S. Hilaire, V. Plujko, M. Avrigeanu, O. Bersillon, M. Chadwick, T. Fukahori, Z. Ge, Y. Han, S. Kailas, J. Kopecky, V. Maslov, G. Reffo, M. Sin, E. Soukhovitskii, and P. Talou, Nucl. Data Sheets **110**, 3107 (2009).

[36] M. Verpelli and R. Capote, International nuclear data committee, Update of RIPL nuclear levels segment, Tech. Rep. No. INDC(NDS)-0702 (IAEA, Vienna, 2015), https://www-nds.iaea.org/publications/indc/indc-nds-0702/.

[37] A. Gilbert and A. G. W. Cameron, Can. J. Phys. **43**, 1446 (1965).

[38] F. Bečvář, Nucl. Instrum. Methods Phys. Res., Sect. A **417**, 434 (1998).

[39] A. Koning and J. Delaroche, Nucl. Phys. A **713**, 231 (2003).

[40] J. Raynal, Notes on ECIS94, Tech. Rep. No. CEA-N-2772 (CEA, Saclay, 1994).

[41] J. Kopecky and M. Uhl, Phys. Rev. C **41**, 1941 (1990).

[42] T. Kibédi, T. Burrows, M. Trzhaskovskaya, P. Davidson, and C. Nestor, Nucl. Instrum. Methods Phys. Res., Sect. A **589**, 202 (2008).

[43] L. Landau, in *Collected Papers of L. D. Landau* (Pergamon, Oxford, 1965).

[44] A. Chebboubi, O. Serot, G. Kessedjian, O. Litaize, A. Blanc, D. Bernard, H. Faust, S. Julien-Laferrière, U. Köster, A. Letourneau, T. Materna, O. Méplan, P. Mutti, M. Rapala, and C. Sage, EPJ Web Conf. **146**, 04063 (2017).

[45] T. Wang, G. Li, L. Zhu, Q. Meng, L. Wang, H. Han, W. Zhang, H. Xia, L. Hou, R. Vogt, and J. Randrup, Phys. Rev. C **93**, 014606 (2016).

[46] M. Jandel, B. Baramsai, T. Bredeweg, A. Couture, A. Favalli, A. Hayes, K. Ianakiev, M. Iliev, T. Kawano, S. Mosby, G. Rusev, I. Stetcu, P. Talou, J. Ullmann, D. Vieira, C. Walker, and J. Wilhelmy, Nucl. Instrum. Methods Phys. Res., Sect. A **882**, 105 (2018).

[47] C. Michelagnoli, A. Blanc, E. Ruiz-Martinez, A. Chebboubi, H. Faust, E. Froidefond, G. Kessedjian, M. Jentschel, U. Köster, P. Mutti, and G. Simpson, EPJ Web Conf. **193**, 04009 (2018).

Report_SANDA_Deliverable_D2.12_Julien-Laferriere_2020a

Fission fragments observables measured at the LOHENGRIN spectrometer

S. Julien-Laferrière[1,2], *L.* Thombansen[2], *G.* Kessedjian[2], *A.* Chebboubi[1], *O.* Serot[1], *C.* Sage[2,*], *O.* Méplan[2], *M.* Ramdhane[2], *O.* Litaize[1], *J.* Nicholson[1], *D.* Bernard[1], *U.* Köster[3], *P.* Mutti[3], *T.* Materna[4], and *M.* Rapala[4]

[1]CEA, DEN, DER, SPRC, LEPh, Cadarache center, F-13108 Saint-Paul-lez-Durance, France
[2]LPSC, Université Grenoble-Alpes, CNRS/IN2P3, F-38026 Grenoble Cedex, France
[3]Institut Laue-Langevin, F-38042 Grenoble Cedex 9, France
[4]CEA, DSM, IRFU, SPhN, LEARN, Saclay center, F-91191 Gif-sur-Yvette, France

Abstract. Nuclear fission yields are key data for reactor studies, such as spent fuel inventory or decay heat, and for understanding fission process. Despite a significant effort allocated to measure fission yields during the last decades, the recent evaluated libraries still need improvements in particular in the reduction of the uncertainties. Moreover, some discrepancies between these libraries must be explained.

Additional measurements provide complementary information and estimations of experimental correlations, and new kinds of measurements enable to test the models used during the nuclear data evaluation process. A common effort by the CEA, the LPSC and the ILL aims at tackling these issues by providing precise measurements of isotopic and isobaric fission yields with the related variance-covariance matrices. Additionally, the experimental program involves a large range of observables requested by the evaluations, such as kinetic energy dependency of isotopic yields and odd-even effect in order to test the sharing of total excitation energy and the spin generation mechanism. Another example is the complete range of isotopic distribution per mass that allows the determination of the charge polarization, which has to be consistent for complementary masses (pre-neutron emission). For instance, this information is the key observable for the evaluation of isotopic yields. Finally, ionic charge distributions are indirect measurements of nanosecond isomeric ratios as a probe of the nuclear de-excitation path in the (E^*, J, π) representation.

Measurements for thermal neutron induced fission of ^{241}Pu have been carried out at the ILL in Grenoble, using the LOHENGRIN mass spectrometer. Methods, results and comparison to models calculations will be presented corresponding to a status on fission fragments observables reachable with this facility.

1 Introduction

An accurate knowledge of fission data in the actinide region is important for studies of innovative nuclear reactor concepts. Fission yield measurements supply experimental data to put constraints on fission models and improve their predictive power. In the framework of nuclear data evaluation, these models are indeed necessary to increase the consistency and the precision of the libraries. Despite a real effort on fission yields measurements, current evaluated data still need some improvements on different aspects, such as for instance the uncertainties reduction and the estimation of covariance matrices. A special focus on the heavy and symmetry mass regions is important, since it is where the discrepancies between models (or evaluations) and the few experimental data are mainly observed.

A collaboration between the CEA, the LPSC and the Institute Laue Langevin (ILL) is involved in an experimental program using thermal neutrons of the ILL and the LOHENGRIN spectrometer to study the fission process. We developed different methodologies to obtain absolute isobaric and isotopic yields with the estimation of the covariance matrices associated to the measurements. Besides,

the measurement of different observables combined with a comparision with simulation codes such as FIFRELIN [1] enable to get insight data to better understand the fission process. Isomeric ratios can give an indirect information on the fragments spin ditribution, and their kinetic energy dependency enlights on the validity of the models in use. An exhaustive set of isotopic yields per mass enables the charge polarisation estimation, which has to be consistent between complementary masses. A final example of such indirect data measured by our collaboration is the extraction of nanosecond isomeric ratios determined from the ionic charge distributions per isotope.

2 The LOHENGRIN spectrometer

The LOHENGRIN mass spectrometer [2] is a nuclear physics instrument from the ILL research reactor facility which allows to study fragment distributions from thermal neutron induced fission with a very high mass resolution ($\Delta A/A \approx 1/400$). A fissile actinide target is placed close to the reactor core, in a thermal neutron flux reaching 5×10^{14} neutron.cm^{-2}.s^{-1}.

Fission fragments emerge from the target with an ionic charge distributed around an average ionic charge state of

---

*e-mail: sage@lpsc.in2p3.fr

about 20 to 23. Those fragments that are emitted along the beam tube axis undergo a horizontal deflection in a magnetic field, directly followed by a vertical deflection in an electric field. These combined fields separate ions according to their A/q and E_k/q ratios, with A, q and E_k the mass, ionic charge state and kinetic energy of the ions respectively. These ratios can be achieved with different triplets (A, E_k, q) leading to a possible degeneracy.

At the spectrometer exit, different detection systems can be installed, such as a dual anode Frisch grid ionisation chamber for mass yield measurements, or two clovers of four high purity Germanium crystals that are used with an additional magnet whose aim is to focus the ion beam. A schematic view of the spectrometer is shown in Fig. 1.
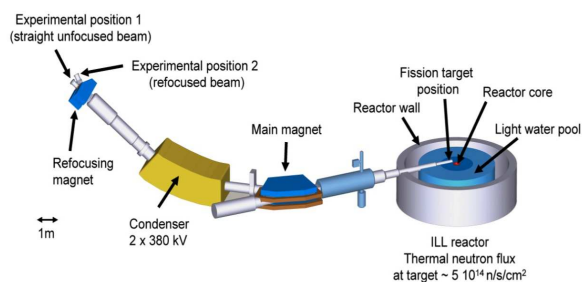
Figure 1. Schematic overview of the LOHENGRIN spectrometer at ILL.

3 Mass and isotopic yields measurements of the ^{241}Pu(n$_{th}$,f) reaction

The first goal of our collaboration measurement campaign consists in the precise measurements of mass, isotopic and isomeric yields, with a control of the systematic effects and the determination of the covariance matrices associated to the analyses. For these observables, their dependency with fission fragment kinetic energy increases significantly the retrieved information on the fission process.

3.1 Mass yields

Isobaric yields are obtained from experimental position 1 (see Fig. 1) after an integration over the kinetic energy and the ionic charge distributions of the count rates measured with the ionisation chamber. A new measurement method and consequent analysis path have been developed and are detailed in Ref. [3–6]. Among the special features of this method are the self-normalisation of our data and the calculation of the experimental covariance matrices. Provided that all the heavy mass rates are measured, it is possible to self-normalise the data by defining to 100% the sum of the whole heavy peak yields. As a consequence, these new measurements are independent from another experiment or assessment and may be compared directly with the existing data and evaluations.

The results for ^{241}Pu(n$_{th}$,f) are shown in Fig. 2, where they are compared to the JEFF-3.3 [7] and ENDF/B-VII.1 [8] libraries. The whole heavy peak and an important part

of the light one were measured. Our results are slightly higher than the libraries for the light mass region, and a structure around mass 140 is observed in the heavy region. Our experimental uncertainties are around 5% on average and below the ones indicated in the two libraries.
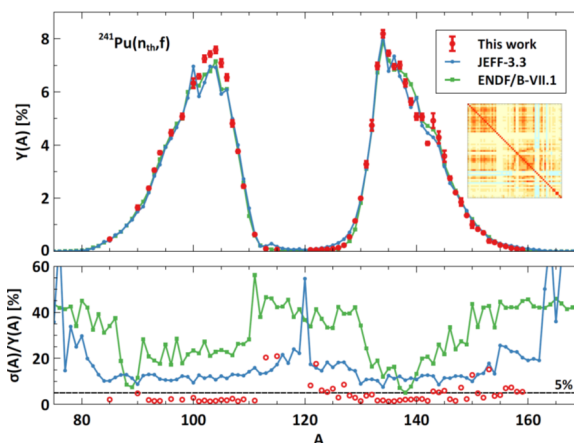
Figure 2. Mass yields for the ^{241}Pu(n$_{th}$,f) reaction and their relative uncertainties.

3.2 Isotopic yields

Isotopic and long-lived isomeric (few μs to ms) fission yields are measured by gamma spectrometry. Experimental position 2 (see Fig. 1) is now used.The ion beam is deposited on a moving tape inside a vacuum chamber and a cumulative measurement with duration of about 30 min per point over the ionic charge distribution is achieved. The tape moves at the end of the measurement to clean the environment and start a new measurement. After corrections of the Bateman equations and the estimation of the contribution of the isotopes from the tape only, we obtain the isotopic distributions per mass. As for the mass yields, a particular effort is made on the determination of the systematic uncertainties and the covariance associated to the measurement process.

Fig. 3 shows a scheme summarizing the measurement procedure and the isotopic yields obtained for the chains 137 and 139 are shown in Fig. 4, along with the covariance matrices. It is important to note that the uncertainties are dominated by the nuclear structure data. Thus current yields measurements can be improved by increasing the nuclear structure knowledge. Fig. 5 helps to understand the construction of the experimental covariance matrix at the main steps of the analysis as illustration of the uncertainty propagation effects.

4 Indirect data measurements

Besides isobaric and isotopic yields, other fission observables are achievable with the LOHENGRIN spectrometer and give important complementary information for the study of the fission process. The kinetic energy dependency of the isotopic and isomeric yields has been already
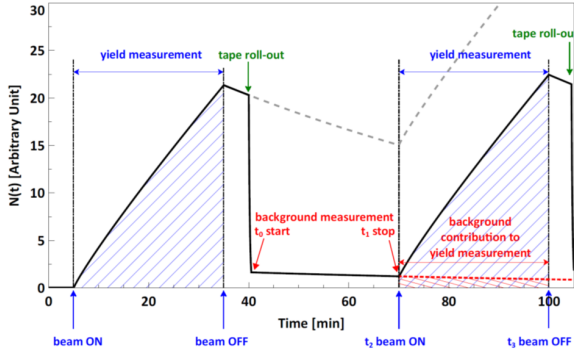
Figure 3. Evolution of a typical isotopic yields measurement procedure.
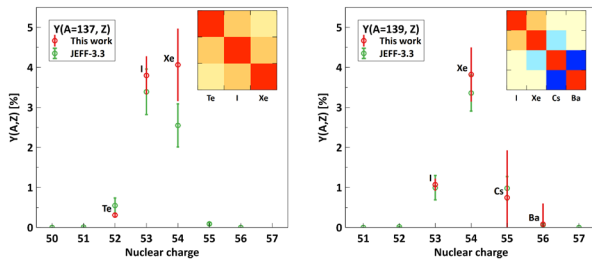
Figure 4. Isotopic yields of the ^{241}Pu(n$_{th}$,f) reaction for masses 137 and 139, along with the experimental covariance matrices
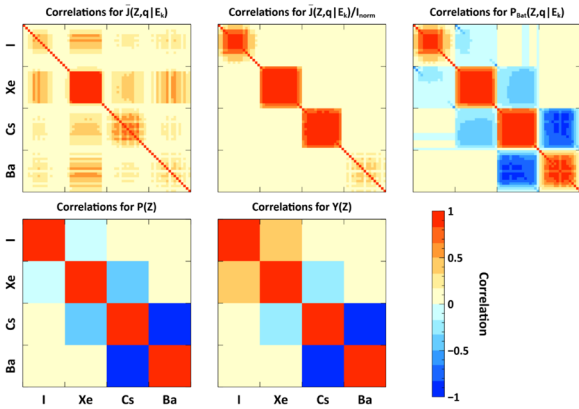
Figure 5. The correlation matrix for mass 139 at different steps of the analysis. 1st step: average on the different gamma rays. 2nd step: Division by I^{norm}. 3rd step: Independent production rate calculation. 4th step: sum over the ionic charges. 5th step: absolute yields after self normalisation.

discussed in ref. [9, 10]. This paper will focus on the description of the charge polarisation and the estimation of nanosecond isomeric ratios.

4.1 Nuclear charge polarisation

The charge polarisation can be extracted from the combination of the isotopic and isobaric yields measurements. It is defined as the difference between the measured mean

nuclear charge and the fragment nuclear charge in the Unchanged Charge Density (UCD) hypothesis.

Fig. 6 shows the measured charge polarisation for the concerned masses in the heavy peak region, compared with the JEFF-3.1.1 library and previous experimental data from Schillebeeckx et al. [11]. We observe a good agreement for the mass 130 and around mass 140, but a strong structure appears for the masses 132, 136 and 138. Complementary measurements on the neighbouring masses are planned by the collaboration to better understand this phenomenon.
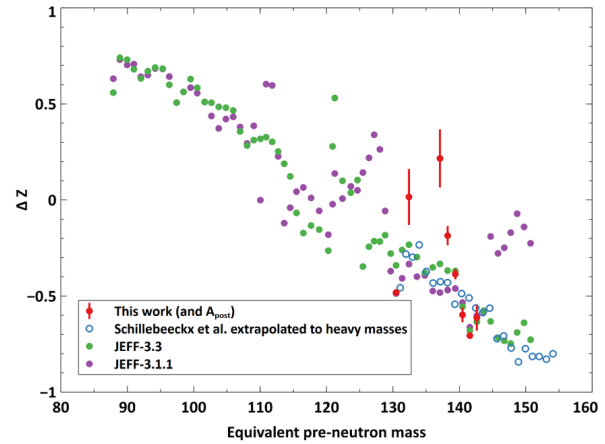
Figure 6. Charge polarisation measured in the heavy peak region as a function of the pre-neutron mass, compared with the JEFF-3.1.1 library and previous experimental data from Schillebeeckx et al. [11].

4.2 Nanosecond converted isomeric ratios

Indirect measurements of nanosecond IR's can be determined from the ionic charge distributions [12, 13]. The method consists in the deconvolution of the ionic charge distribution per isotope obtained by gamma spectrometry after correction from Bateman equations. The converted isomeric ratio (CIR) is defined as the converted isomer population over the total ionic population (converted and unconverted).

$$CIR = \frac{N(A, Z, m \to e^-)}{N(A, Z, GS) + N(A, Z, m \to \gamma) + N(A, Z, m \to e^-)} \quad (1)$$

According to the statistical models from H. Betz [14], we assume that the ionic charge distribution associated to the unconverted population follows a Gaussian distribution due to the charge equilibrium in the cover of the target (a Nickel foil in this work). A deviation from this Gaussian distribution indicates a charge modification due to the conversion from ps and ns isomers to groundstate (see Fig. 7). In most of the cases the deconvolution is achieved using two Gaussian distributions and a Monte Carlo simulation to deduce the CIR in order to consider the covariance terms between the Gaussian integrals. CIR measurements for ^{241}Pu(n$_{th}$,f) and ^{233}U(n$_{th}$,f) are shown in Fig. 8 and compared to FIFRELIN calculations for ^{241}Pu(n$_{th}$,f). We note

Report_SANDA_Deliverable_D2.12_Julien-Laferriere_2020b
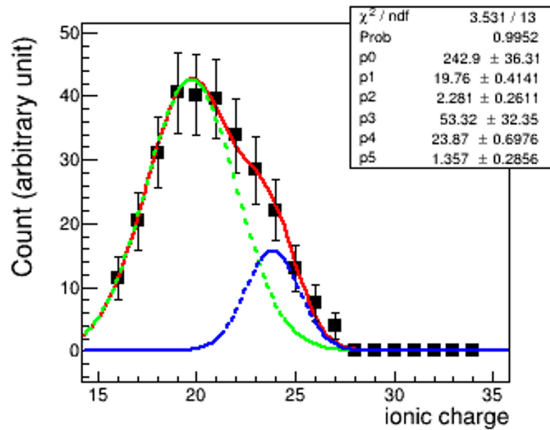
Figure 7. Ionic charge distribution de-convoluted using the Gaussian assumption for the unconverted state according to the Betz model [14]. The blue curve corresponds to the ns isomer contribution.
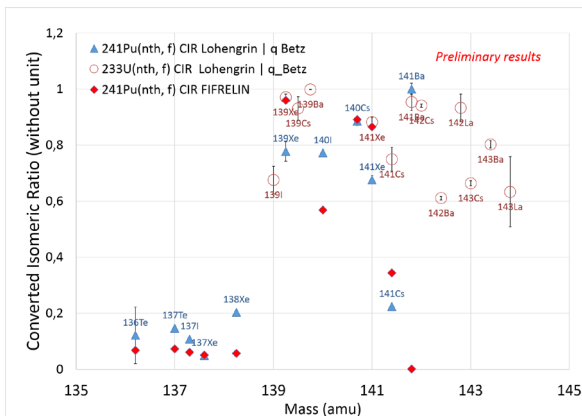
Figure 8. Converted isomeric ratios as a function of the mass induced by the fission of $^{241}Pu(n_{th},f)$ and $^{233}U(n_{th},f)$ in comparison with FIFRELIN calculations.

a good tendency even if some differences have to be explored in details given the assumption used in the analysis or the models considered for the decay cascade calculations. For some nuclei, many isomers and bands have to be taken into account at the limit of the knowledge of the nuclear structure. Then it corresponds to integral measurements used to test the overal decay cascade.

5 Conclusion and perspectives

An experimental program dedicated to precise absolute measurements of isobaric, isotopic and isomeric yields is ongoing using the LOHENGRIN mass spectrometer

at ILL. Recent results concern the ^{241}Pu(n$_{th}$,f) reaction, where a dedicated analysis method with a control of the systematic uncertainties and computation of the covariance matrices was achieved. Interesting indirect data are also measured and dedicated to test the phenomenological models and the assumptions used for the evaluations, through a comparison with calculations using the FIFRELIN code developped at CEA Cadarache. In this frame, nuclear charge polarisation and nanosecond CIR are the main examples of such investigations. Our collaboration plans to continue this measurement program for different fissioning systems, as new measurements and validated models are central in order to progress in the evaluation topic.

Acknowledgements

References

[1] O. Litaize and O. Serot, Eur. Phys. J . A **51**, 177 (2015)
[2] P. Armbruster *et al.*, *Nucl. Instrum. Methods* **139** 213 (1976)
[3] F. Martin *et al.*, Proc. 2nd ANIMMA Conference, June 2011, Ghent (Belgium).
[4] F. Martin *et al.*, Nuclear Data Sheets **119**, 328-330 (2014)
[5] S. Julien-Laferrière *et al.*, EPJ Nucl. Sci. Technol. **4**, 25 (2018)
[6] Y. Gupta *et al.*, Phys. Rev. C **96**, 014608 (2017)
[7] The JEFF-3.1.1 nuclear data library. OECD, NEA, JEFF Report 21, ISBN 92-64-02314-3 (2006).
[8] M. B. Chadwick *et al.*, Nucl. Data Sheets **107**, 2931 (2006)
[9] S. Julien-Laferrière *et al.*, EPJ Web of Conferences **211**, 04004 (2019)
[10] A. Chebboubi *et al.*, Phys. Lett. B **775**, 190-195 (2017)
[11] P. Schillebeeckx *et al.*, Nucl. Phys. A **580**, 15-32 (1994)
[12] T. Rzaca-Urban, J. Genevey, T. Materna *et al.*, Phys. Rev. C **80**, 064317 (2009)
[13] A. Chebboubi *et al.*, EPJ Web of Conferences **146**, 04021 (2017)
[14] H. D. Betz, Rev. Mod. Phys. **44**, 465-539 (1972)
[15] R. Capote *et al.*, Nucl. Data Sheets **110**, 3107 (2009)

Investigation of fission product isomeric ratios and angular momenta of ^{132}Sn populated in the ^{241}Pu(n$_{th}$,f) reaction

Jehaan Nicholson[1], *Abdelhazize* Chebboubi[1,*], *Olivier* Serot[1], *Grégoire* Kessedjian[2], *Yung Hee* Kim[3], *Ulli* Köster[3], *Olivier* Litaize[1], *Olivier* Méplan[2], and *Christophe* Sage[2], and *Mourad* Ramdhane[2]

[1]CEA, DEN, DER, SPRC, Cadarache, Physics Studies Laboratory, 13108 Saint-Paul-lès-Durance, France
[2]LPSC, Université Grenoble-Alpes, CNRS/IN2P3, 38026 Grenoble Cedex, France
[3]Institut Laue-Langevin, 38042 Grenoble Cedex 9, France

Abstract. During an experimental campaign performed at the LOHENGRIN recoil spectrometer of the Institut Laue-Langevin (ILL), a kinetic energy dependence of ^{132}Sn fission product isomeric ratio (IR) has been measured by inducing thermal fission of ^{241}Pu. The IRs are deduced using gamma ray spectrometry in coincidence with the ionisation chamber. To interpret these data, we use the FIFRELIN Monte-Carlo code to simulate the de-excitation of the fission fragments. Combining the IRs with the FIFRELIN calculations, the angular momentum distribution with kinetic energy of the doubly magic nucleus of ^{132}Sn was deduced. This will be compared with the angular momentum distribution obtained for the reaction ^{235}U(n$_{th}$,f) for ^{132}Sn.

1 Introduction

The past decade has seen a growing energy need and thus a renewed interest in nuclear energy. Nonetheless, to make the new reactors more safe, the existing technology needs to be improved and the challenge for new and innovative fuel must be overcome. Furthermore, a precise understanding of the fission process is a noteworthy challenge faced by nuclear physicists even though eight decades have passed since its discovery in 1939 [1, 2]. Many different models and hypotheses such as the liquid drop model, shell model etc. have been developed to explain and reproduce the experimental data obtained as well as to improve the understanding of fission. However, the angular momenta of the fission fragments are a poorly known quantity. Angular momenta of fission fragments are a component of the phenomenological model used to assess nuclear observables used in applications as prompt gammas and neutrons. This angular momentum can be estimated by using models, see for example Ref. [3], or through direct measurements, see Ref. [4] and references therein. On the other hand, one can study indirectly the angular momenta of the fission fragments by measuring the isomeric ratios of the fission fragments [5–7].

---

*e-mail: Abdelhazize.CHEBBOUBI@cea.fr

Report_SANDA_Deliverable_D2.12_Nicholson_2021b

2 Experiment

The experiment was conducted at the LOHENGRIN recoil spectrometer [8] at the Institut Laue-Langevin (ILL) [9]. The LOHENGRIN recoil spectrometer was built in the 1970s and is one of the key instruments at the ILL to carry out experiments for nuclear physics and nuclear data. The LOHENGRIN recoil spectrometer enables us to study the mass, charge and kinetic energy distribution of the fission products. These fission products are obtained by exposing a fissile or fertile target to a thermal neutron flux of about 5×10^{14} n/cm²/s near the core of the ILL high-flux reactor. The total length of LOHENGRIN is 23 m and has a high mass resolution (A/ΔA $\cong$400) [10], which is dependent on target size. By using the electric and magnetic fields of LOHENGRIN, fission products of interest are extracted and brought to the detection area. These fields are perpendicular to each other and have focussing properties in their respective planes.
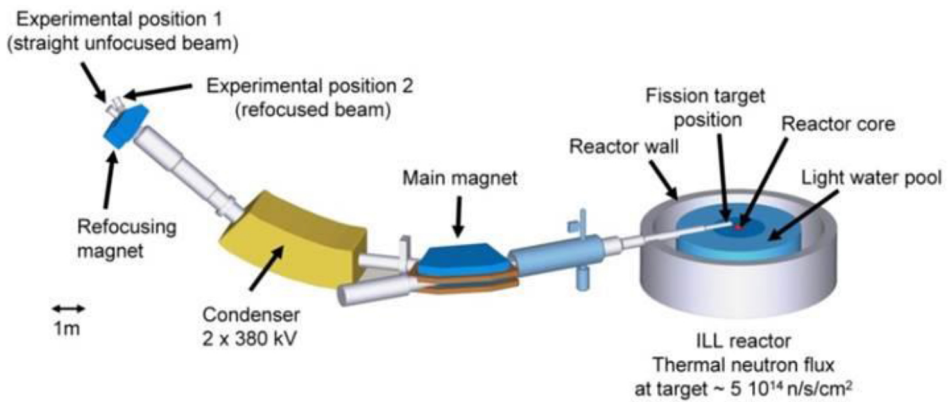
Figure 1. Schematic of the LOHENGRIN mass spectrometer showing the dipole magnet in blue (centre) and the electrostatic condenser in yellow. They are used to generate the electric and magnetic fields, which are used to select and divert the charged fission products.

For this experiment, we used ^{241}Pu (39.9 μg/cm²) as the target nuclei. By varying the electric and magnetic fields, the desired fission products are selected by the A/q and E_k/q ratio, where A is the desired mass of the fission product, q is the ionic charge and E_k its kinetic energy. As can be seen from Fig. 1, there are two experimental positions present. At experiment position 1, the beam has an energy dispersion of 7.2 cm per 1% energy difference, whereas at position 2, the beam is refocussed in the energy axis using the RED magnet [11] and, hence, the particle flux density is increased by up to a factor of seven [10] as compared to position 1. In our experiment, the detectors were set up at position 2. The detection setup consists of an ionisation chamber and two HPGe clover detectors with four germanium crystals each. This is depicted in Figure 2.

The extracted fission products are then implanted in the Al foil at the top of the ionisation chamber. The gamma rays, emitted by internal transition (IT) of the isomeric state and after the β- decay of the ground state are detected using the two clover detectors. By using LOHENGRIN, ^{132}Sn was extracted at ionic charges 20 and 24 respectively with kinetic energy ranging from 57 MeV to 84 MeV.

Report_SANDA_Deliverable_D2.12_Nicholson_2021b
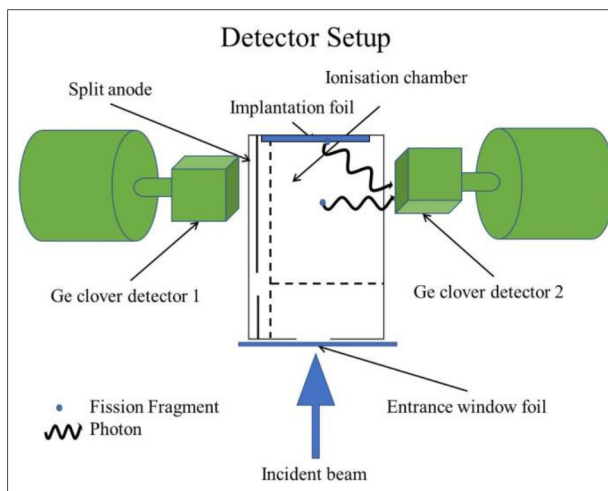
Figure 2. Detector setup showing the two HPGe clover detectors in green and the split-anode ionisation chamber in between them. The implantation foil is placed at the top of the ionisation chamber to trap the fission products.

3 Isomeric ratios from experiments

Isomeric ratios (IR) are defined as ratio of the production rate (P_i) of one isomeric state to the sum of the production rates of all the isomeric states and the ground state (GS).

$$IR = \frac{P_i}{\sum P_i + GS} \tag{1}$$

3.1 The analysis

^{132}Sn has one microsecond isomeric state at 4848.5 keV having $J^\pi = 8^+$ with a half-life of 2.08 μs [12]. The analysis was carried out off-line. To analyse the gamma rays originating from the isomeric state, a coincidence spectrum was generated. The time coincidence window was set to 20 μs. The coincidence was created between the ionisation chamber and the HPGe clover detectors. By using the coincidence method to generate a spectrum, we are able to reduce the gammas originating from room background and beta decays and gammas from β- decay of the ground state of the parent nucleus (^{132}In). Thus, we obtain a clean spectrum for the gamma rays originating from the microsecond isomeric state of ^{132}Sn as seen in the Fig. 3. For the measurement of the gamma rays originating from the β- decay of the ground state (^{132}Sn), the ungated spectrum was used.

The gamma spectrum was analysed using the TV gamma spectrum analyser program [13]. The intensities of the gamma rays were obtained from literature [12] and the efficiencies for the germanium detectors were obtained from simulations validated with experimental data. To calculate the IR from the counts obtained from the gamma spectra, firstly, we have to calculate the production rates of the isomeric state as well as the ground state. To do this, the Bateman equations need to be solved. Along with this, corrections for the decay during flight also need to be taken into account; this is due to the fact that the distance between target and the experimental focal plane is 23 m. To accurately determine the production rates and the IR along with their respective uncertainties, a Monte-Carlo method [5, 14] is being used. This

Monte-Carlo Code (MCC) is used as compared to the analytical method as there are quite a few parameters involved in different corrections, which need to be added. Hence trying to propagate and calculate their uncertainties analytically would be a complex task.
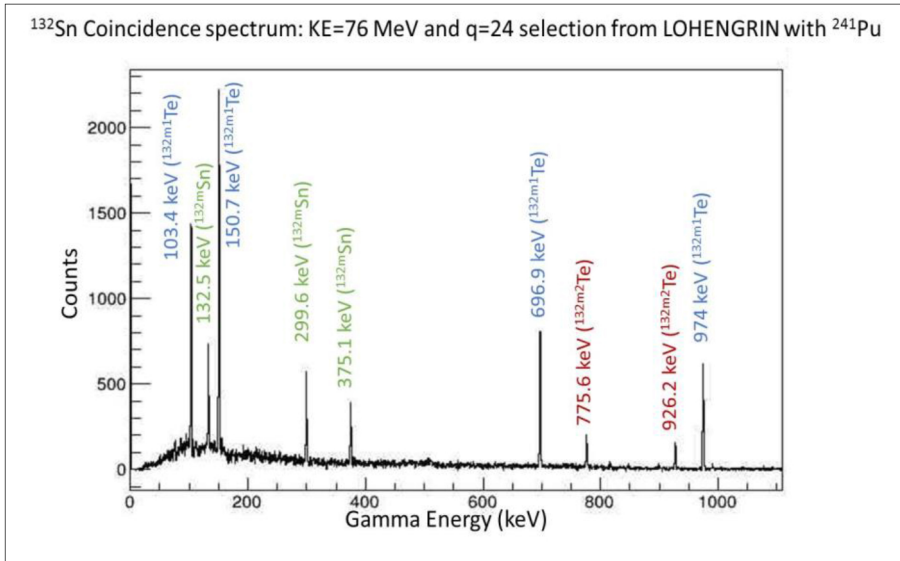
Figure 3. Gated Spectrum showing the three gamma rays of interest (in green) from the ^{132}Sn isomeric state (IS). Gamma rays from the two ISs of ^{132}Te are also observed in this spectrum.

As input to the MCC, one must provide the half-life of the states (ground and isomeric), counts and the error on counts which are extracted using TV gamma spectrum analyser, detection efficiency, the gamma intensities and the normalisation factor for the gamma intensities, the branching ratio, kinetic energy selected by LOHENGRIN and the flight path length. The MCC then calculates the average number of disintegrations (N_d), the production rates and the isomeric ratios along with their respective uncertainties. One can also obtain sensibility plots as well as covariance matrices from the MCC.

In the MCC, N_d is calculated for each of the gamma rays (N_{di}) arising from a particular state, these N_{di} are then used to calculate the mean N_d. The χ^2 test is used to verify whether a 90% level of confidence is achieved. If not, progressively, uncertainty is added [15] and the N_d is recalculated to achieve the test criteria. Thus, a final mean value of the N_d along with its uncertainty is obtained. The systematic uncertainties account for less than 5%, whereas the statistical uncertainties go as high as 50%.

The beamtime had a span of ten days and hence, not all the measurements were performed consecutively or even on the same day. For this reason, we must take into account the target evolution. To see the target evolution, several energy scans were carried out throughout the experiment schedule. The shift in the mean value of the kinetic energy between the first and the last experimental days is equal to (4.6 ± 1.0) MeV. It should be noted that the evolution of the mean kinetic energy was linear with a slope of (-0.52 ± 0.09) MeV/day. For each kinetic energy selected with the LOHENGRIN spectrometer, IRs are measured. By combining all the experimental data (weighted by the kinetic energy distribution) the mean IR can be derived and is equal to 0.0719 ± 0.0016. It should be noted that covariance was not taken into account for the uncertainty propagation.
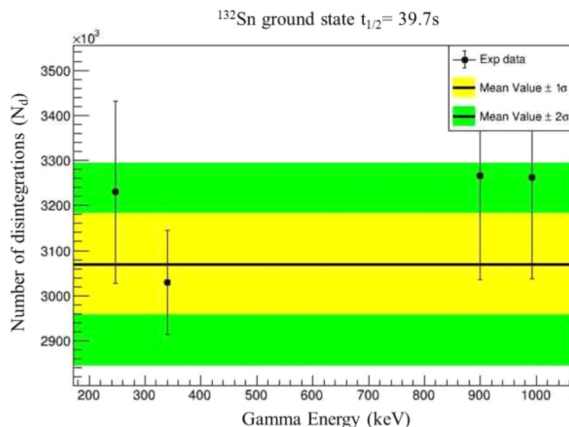
Figure 4. Number of disintegrations calculation using the MCC for GS for 72 MeV and q=24 selection of LOHENGRIN.
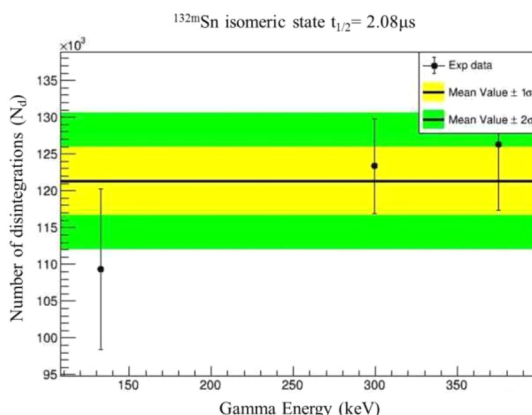
Figure 5. Number of disintegrations calculation using the MCC for IS for 72 MeV and q=24 selection of LOHENGRIN.

4 Spin extraction using FIFRELIN

FIssion FRagment Evaporation Leading to an Investigation in Nuclear data (FIFRELIN) [16] is a Monte-Carlo code developed at CEA. This code simulates the fission process and gives information on fission observables such as prompt neutrons, gammas, neutron multiplicity. For this work, this code has only been used to carry out the de-excitation simulation of the nuclei of interest (^{132}Sn). The inputs provided for this code are the mass number (A), the atomic number (Z), excitation energy (E^*) and spin along with parity (J^{π}). It also requires additional files from the RIPL-3 2015 [17, 18] library to get information on the nuclear levels and the gammas and electrons emitted at lower energies. Additional models are also required such as the Composite Gilbert-Cameron Model (CGCM), which is propositioned in RIPL-3 [17] for nuclear level densities, Back Shifted Fermi Gas Model (BSFGM) for spin cut-off and the Enhanced General Lorentzian (EGLO) model [19] for the gamma strength functions. The BRICC code [20] is used to calculate the internal conversion coefficients. FIFRELIN

uses these input libraries and assumes that the experimental level scheme provided in the RIPL-3 2015 file is complete up to cut-off energy (E_{cut}). After this E_{cut}, it is assumed that the experimental level scheme is incomplete and this is then filled by FIFRELIN using the CGCM model. The BSFGM is used to attribute a J^π value to these new levels and the EGLO model is used to get the gammas and their respective intensities originating from these levels. The probability to emit neutrons are obtained from the neutron transmission coefficients which are derived from an optical model; the Koning-Delaroche global neutron optical model potential [21] but in our case, no neutrons are emitted as the simulations were run below neutron separation energy.
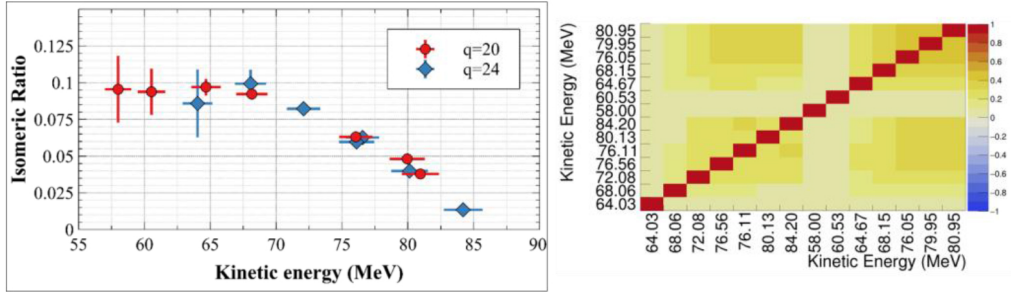
Figure 6. Isomeric Ratio of ^{132}Sn from thermal neutron induced fission of ^{241}Pu measured at two different ionic charge selections (left) and the associated covariance matrix (right). The kinetic energies are corrected from the relative evolution of the energy loss during the experimental campaign.

Once the input parameters, A, Z, E^* and J^π are provided, a cascade can start. The above-mentioned models and experimental level schemes are used to calculate the isomeric ratio for a particular E^* and J^π combination. The E^* has a range starting at the energy of the isomeric state up to the neutron separation energy. For each excitation energy, a range J^π of values ($0^\pm$ to $30^\pm$) is given. For each of these J^π values, an IR ($IR_{FIF}(E^*, J^\pi)$) is calculated by FIFRELIN. To compare these results with the experimental data, the results are averaged by the equation given below:

$$IR_{FIF}(E^*, J_{rms}) = \sum_J \sum_\pi P(\pi) P(J) IR_{FIF}(E^*, J^\pi) \tag{2}$$

$$\text{where } P(J) \propto (2J + 1) \exp\left(-\frac{\left(J + \frac{1}{2}\right)^2}{J_{rms}^2}\right) \tag{3}$$

$$\text{and } P(\pi) = P(\pm 1) = \frac{1}{2} \tag{4}$$

The Likelihood method is used to adjust the spin cut-off (J_{rms},) which in that case is a free parameter

$$L(E^*, J_{rms} \mid E_k) \propto \exp\left(-\frac{\left(IR_{exp}(E_k) - IR_{FIF}(E^*, J_{rms})\right)^2}{2\left(\sigma_{exp}^2, \sigma_{FIF}^2\right)}\right) \tag{5}$$

where, $IR_{exp}(E_k)$ and σ_{exp} are the isomeric ratios and their uncertainty obtained from the experiments that is dependent on the selected kinetic energy from LOHENGRIN. σ_{FIF} is the uncertainty obtained from FIFRELIN.

Report_SANDA_Deliverable_D2.12_Nicholson_2021b

5 Results and conclusion

Combining the FIFRELIN calculations with the experimental results, we were able to extract the J_{rms} value as a function of kinetic energy. Figure 7 depicts the results from this work, which have been compared to the results obtained by using a ^{235}U target [5]. It can be seen that the J_{rms} value obtained from two different fissioning systems are quite similar. Also for this work, one can observe a flat plateau-like region at lower kinetic energies. Further experiments and calculations need to be carried out to explain this phenomenon. Experimental results from this work have been further compared with the calculations using the Madland-England (M.E.) model and the GEF code. This can be seen in Table 1. The M.E. model uses the assumption that the isomeric ratio is only dependant on the spin of both the ground state and the isomeric state. Furthermore, it works on the supposition that all the fission fragments are characterised by a spin cut-off value of (7.5±0.5) h, which gives an isomeric ratio of 0.642±0.039 for ^{132}Sn (M.E. (a)). By using the isomeric ratio from this work, which is 0.0719±0.0016, a J_{rms} of 2.8±0.1 (M.E. (b)) is obtained from the M.E. model. We clearly observe a mismatch between the experimental results and those obtained from the M.E. model for ^{132}Sn.

Table 1. Comparison of results: In M.E. (a), $\overline{J_{rms}}$ is set to 7.5 h and the IR is calculated by using M.E. model. In M.E. (b), the IR is set equivalent to our experimental result and the $\overline{J_{rms}}$ is calculated using the same model.

Experiments	$\overline{IR}$	$\overline{J_{rms}}$ ($\hbar$)
This work (^{241}Pu)	0.0719±0.0016	4.8±0.1
^{235}U [5]	0.054±0.006	4.7±0.2
Models		
Madland-England (a)	0.642±0.039	7.5±0.5
Madland-England (b)	0.0719±0.0016	2.8±0.1
GEF [22]	0.234	6.65±0.03
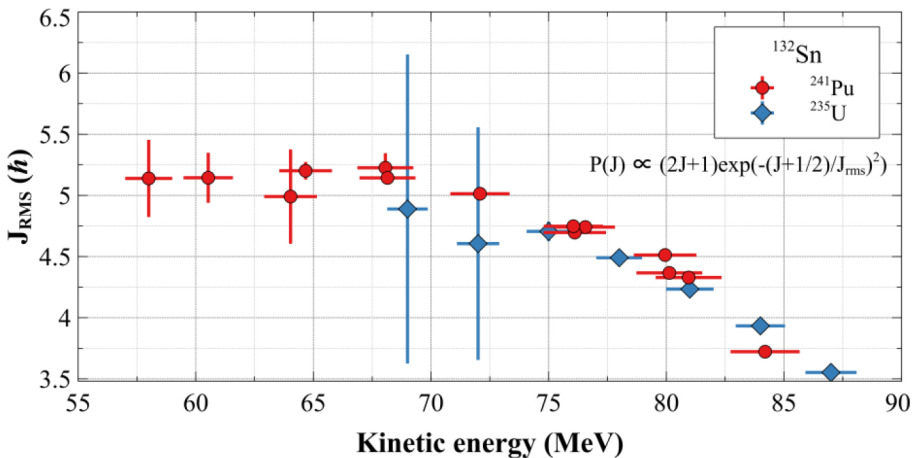
Figure 7. Spin of ^{132}Sn and its dependence on kinetic energy using ^{241}Pu and ^{235}U targets. The kinetic energies are corrected from the relative evolution of the energy loss during the experimental campaign.

Report_SANDA_Deliverable_D2.12_Nicholson_2021b

In conclusion, the dependence of the isomeric ratios of the fission products on their kinetic energy was obtained. Using statistical analysis, along with FIFRELIN calculations involving level density models, gamma strength functions, spin cut-off models and internal conversion coefficients, we were able to determine the J_{rms} value for each of the isomeric ratios obtained. Furthermore, it can be observed that the J_{rms} values for two different fissioning systems are quite similar and follow a similar trend. For nuclei such as ^{132}Sn, the results from the experiments should be taken into account for the nuclear data evaluations instead of using codes or models to compute them. In this same experimental campaign, experiments were carried out on other isotopes of Sn as well. It would be very interesting to see how the J_{rms} value changes with change in mass for the same element.

Raw data of this experiment are available via ref. [23].

References

[1] O. Hahn, F.W. Strassmann, Naturwissenschaften **27**, 11 (1939)

[2] L. Meitner, O.R. Frisch, Nature **142**, 239 (1939)

[3] D. Madland, T. England, Nuclear science and Engineering **64**, 859-865 (1977)

[4] D. Tarrío, L.S. Leong, L. Audouin, I. Duran, C. Paradela, et al., Nuclear Instruments and Methods in Physics Research A **743**, 79-85 (2014)

[5] A. Chebboubi, G. Kessedjian, O. Litaize, O. Serot, H. Faust, D. Bernard, A. Blanc, U. Köster, O. Méplan, P. Mutti, C. Sage, Physics Letters B **775**, 190-195 (2017)

[6] A. Al-Adili, V. Rakopoulos, A. Solders, European Physical Journal A **55**, 61 (2019)

[7] V. Rakopoulos, M. Lantz, S. Pomp, A. Solders, A. Al-Adili, L. Canete, T. Eronen, A. Jokinen, A. Kamkainen, A. Mattera, I.D. Moore, D.A. Nesterenko, M. Reponen, S. Rinta-Antila, A. de Roubin, M. Vilén, M. Österlund, H. Penttilä, Physical Review C **99**, 014617 (2019)

[8] P. Armbruster, M. Asghar, J.P. Bocquet, R. Decker, H. Ewald, J. Greif, E. Moll, B. Pfeiffer, H. Schrader, F. Schussler, G. Siegert, H. Wollnik, Nuclear instruments and Methods **139**, 213-222 (1976)

[9] "About ILL; What is The ILL" Institut Laue-Langevin, [Online]. Available: https://www.ill.eu/about-ill/what-is-the-ill/

[10] "PN1 Fission-product spectrometer; PN1 characteristics" [Online]. Available: https://www.ill.eu/users/instruments/instruments-list/pn1/characteristics/

[11] G. Fioni, H.R. Faust, M. Gross, M. Hesse, P. Armbruster, F. Gönnenwein, Nuclear Instruments and Methods in Physics Research A **332**, 175-180 (1993)

[12] Y. Khazov, A.A. Rodionov, S. Sakharov, B. Singh, Nuclear Data Sheets **104**, 497-790 (2005)

[13] A. Fitzler, *Program TV,* Cologne: Institute for Nuclear Physics

[14] A. Chebboubi, *Contribution à l'étude de la fission nucléaire : de LOHENGRIN à FIPPS*, PhD thesis from Université de Grenoble (2015)

[15] S. Julien-Laferrière, A. Chebboubi, G. Kessedjian, O. Serot, EPJ Nuclear Sci. Technol., **4**, 25 (2018)

[16] O. Litaize, O. Serot, L. Berge, The European Physical Journal A **51**, 177 (2015)

[17] R. Capote, M. Herman, P. Oblozinsky, P.G. Young, S. Goriely, T. Belgya, A.V. Ignatyuk, A.J. Koning, S. Hilaire, V.A. Plujko, M. Avrigeanu, O. Bersillon, M. B. Chadwick, T. Fukahori, Z. Ge, Y. Han, S. Kailas, J. Kopecky, V.M. Maslov, G. Reffo, M. Sin, E. Sh. Soukhovitskii, P. Talou, Nuclear Data Sheets **110**, 3107-3214 (2009)

[18] M. Verpelli and R. Capote, "Structure of RIPL discrete level library files," [Online]. Available: https://www-nds.iaea.org/RIPL-3/levels/levels-readme.html

[19] J. Kopecky, M. Uhl, Physical Review C **41** (1990)

[20] T. Kibédi, T.W. Burrows, M.B. Trzhaskovskaya, P.M. Davidson and C.W. Nestor Jr, Nuclear Instruments and Methods in Physics Research A **589**, 202-229 (2008)

[21] A.J. Koning, J.P. Delaroche, Nuclear Physics A **713**, 321-310 (2003)

[22] K.H. Schmidt, B. Jurado, C. Amouroux and C. Schmitt, Nuclear Data Sheets **131**, 107-221 (2016)

[23] G. Kessedjian, D. Bernard, A. Blanc, A. Chebboubi, H. Faust, Y.H. Kim, U. Köster, O. Litaize, O. Méplan, J.N. Nicholson, M. Ramdhane, C. Sage and O. Serot, ILL, doi:10.5291/ILL-DATA.3-01-640 (2018)